# Assessing the bioavailability of black carbon-derived dissolved organic matter for marine heterotrophic prokaryotes

Pauline Martinot, Catherine Guigue, Sandrine Chifflet, Philippe Cuny, Aude Barani, Morgane Didry, Clara Dignan, Léa Guyomarc'h, Nathalie Pradel, Olivier Pringault, et al.

# Assessing the bioavailability of black carbon-derived dissolved organic matter for marine heterotrophic prokaryotes

Pauline L. Martinot[a, c]*, Catherine Guigue[a, c], Sandrine Chifflet[a], Philippe Cuny[a], Aude Barani[a], Morgane Didry[a], Clara Dignan[b], Léa Guyomarc'h[a], Nathalie Pradel[a], Olivier Pringault[a], France Van Wambeke[a], Cam Tu Vu[c], Xavier Mari[a, c], Marc Tedetti[a, c]

[a] Aix Marseille Université, Université de Toulon, CNRS, IRD, MIO, Marseille, France

[b] Université de Toulon, Aix Marseille Université, CNRS, IRD, MIO, Toulon, France

[c] Water - Environment - Oceanography (WEO) Department, University of Science and Technology of Hanoi (USTH), Vietnam Academy of Science and Technology (VAST), Hanoi, Vietnam

* Corresponding author; pauline.martinot@mio.osupytheas.fr

Submitted to *Science of the Total Environment* as a full-length research paper

Revised version, 26 June 2023

## Abstract

Here we investigated the bioavailability of black carbon (BC)-derived dissolved organic matter (DOM) for a natural mixed community of marine heterotrophic prokaryotes. We ran an *in vitro* biodegradation experiment that took place over 3 months and exposed a community of organisms collected in the northwestern Mediterranean Sea (Bay of Marseille, France) to three different soluble fractions of BC prepared in the laboratory from various fossil fuel combustion particulates: standard diesel ($D_{REF}$), oxidized diesel ($D_{REF\text{-}OX}$), and natural samples of ship soot ($D_{SHIP}$). Over the course of the three months, we observed significant decreases in the concentrations of dissolved organic carbon (DOC; from 9 to 21%), dissolved BC (DBC; from 22 to 38%) and dissolved polycyclic aromatic hydrocarbons (d-PAH; from 24 to 64%) along with variability in the growth dynamics and activity of the heterotrophic prokaryotic community. The heterotrophic prokaryotic community exposed to $D_{REF\text{-}OX}$ treatment showed the highest values of respiration and production and the highest cell abundance, associated with the highest decrease in DOC (21%) and d-PAH (64%) concentrations. In the $D_{REF}$ and $D_{SHIP}$ treatments, prokaryotic activity was oriented towards anabolism. $D_{REF}$ treatment led to the highest decrease in DBC concentration (38%). $D_{SHIP}$ treatment, which presented a substantially different d-PAH and dissolved metals content to the other two treatments, showed the lowest decreases in DOC, DBC and d-PAH concentrations, as well as the lowest prokaryotic activity and biomasses. Our results indicate that BC-derived DOM, including the most condensed fraction of this material, is partly bioavailable and therefore likely to be assimilated by marine prokaryotes. The origin of BC/soot deposited at the ocean surface turns out to be a key parameter that dictates the efficiency of biodegradation of its dissolved fraction by heterotrophic prokaryotes.

**Key words:** black carbon, soot, dissolved organic matter, marine prokaryotes, bioavailability, bacterial degradation

## 1. Introduction

Black carbon (BC), also known as soot carbon, is composed of light-absorbing carbonaceous aerosol particles formed during the incomplete combustion of fossil fuels, biofuels, biomass and waste (Masiello, 2004; Velis and Cook, 2021). BC has recently received growing attention due to its impacts on climate and human health (Coppola et al., 2022). Part of the BC produced is emitted to the atmosphere while another fraction remains on the sites of combustion, but both fractions ultimately make their way into aquatic environments through atmospheric deposition and/or river inputs (Bond et al., 2013; Coppola et al., 2018). In aquatic environments, BC is partitioned between particulate and dissolved phases according to its solubility and hydrophobicity (Wagner et al., 2017). Dissolved organic matter (DOM) derived from BC particles, which corresponds to the BC material passing through a filter of pore size between 0.2 and 0.7 µm, encompasses a heterogeneous set of pyrogenic organic molecules issued from the combustion continuum, ranging from non-aromatic, sugar-like compounds to polycondensed aromatic compounds (Wagner et al., 2018). Within this pool of pyrogenic compounds, dissolved BC (DBC) is assumed to be "only" composed of polycondensed aromatic molecules, as assessed by benzenepolycarboxylic acid (BPCA) or chemothermal oxidation (CTO) methods (Wagner et al., 2021).

DBC is now recognized as a major (slow-cycling) component of the global carbon budget (Mannino and Harvey 2004; Dittmar and Paeng, 2009; Jaffé et al., 2013; Bao et al., 2017). DBC is ubiquitous in natural waters and has been reported from inland to oceanic waters, including rivers (Stubbins et al., 2015; Wagner et al., 2019; Jones et al., 2020), streams (Yamashita et al., 2021), submarine groundwater (Seidel et al., 2014), estuaries (Mannino and Harvey, 2004), coastal waters (Coppola et al., 2015; Fang et al., 2017, 2021), the sea surface microlayer (Mari et al., 2014, 2017), open ocean (Ziolkowski and Druffel, 2010; Nakane et al., 2017; Mori et al., 2021) and deep ocean (Dittmar and Koch, 2006;

Stubbins et al., 2012; Coppola and Druffel, 2016). The amount of DBC held in the ocean is estimated at ~12–14 Pg C (Dittmar and Paeng, 2009; Coppola and Druffel, 2016; Wagner et al., 2018; Coppola et al., 2022), which represents ~2% of the total pool of oceanic DOM (~650 Pg C; Moran et al., 2016). However, although DBC is an essential component of the carbon cycle, little is known about its transformation processes and fate in marine waters (Wagner et al., 2018; Qi et al., 2020; Coppola et al., 2022).

DBC has a chemical structure based on polycondensed aromatics compounds that makes it highly photoreactive (Stubbins et al., 2012; 2015), and it is also thought to be considered biorefractory for heterotrophic prokaryotes. However, the actual bioavailability and impact of DBC or BC-derived DOM for/on marine prokaryotes remains to be described. Recent research has reported that BC-derived DOM obtained from leachate experiments on wood charcoal, charred oak and biochar was bioavailable for soil and river microbial consortia (Qi et al., 2020; Bostick et al., 2021; Wagner et al., 2021; Goranov et al., 2022). This biodegradation was attributed to the low-molecular-weight (LMW) organic constituents (biomolecules) of the BC-derived DOM, whereas the true DBC, i.e. its polycondensed aromatic fraction determined by the BPCA method, appeared to be more resistant to microbial degradation (Bostick et al., 2021; Wagner et al., 2021; Yamashita et al., 2022). However, Qi et al. (2020) and Goranov et al. (2022) asserted the aromatic fraction of the BC-derived DOM could be bioavailable and thus get assimilated and integrated into the biomass of the microbial community. They went on to stress that the origin of the pyrogenic material from which the DOM is derived plays an important role in its molecular composition and thus its potential uptake and biodegradation by heterotrophic prokaryotes. Within the spectrum of molecules produced during combustion processes, high-molecular-weight (HMW)/pyrogenic polycyclic aromatic hydrocarbons (PAHs) are likely to be part of the DBC pool (Wagner et al., 2018; Fang et al., 2021), which makes them a relevant parameter for investigating the microbial

assimilation of the aromatic fraction of DOM derived from BC (Liu et al. 2016; Djaoudi et al., 2020). These observations highlight the need for further investigation into the biological reactivity for marine prokaryotes of BC-derived DOM and DBC from BC material of various origins, from biomasses to fossil fuels.

In this context, this study aims to investigate the composition, potential bioavailability and impact of BC-derived DOM for marine heterotrophic prokaryotes. We conducted an *in vitro* biodegradation experiment during 90 days on a prokaryotic assemblage collected in coastal Mediterranean waters exposed to DOM derived from various BC soot originating from fossil fuels. During this 90-day biodegradation experiment, subsamples were taken for the determination of various chemical parameters, including dissolved organic carbon (DOC), DBC (based on the BPCA method), PAHs, chromophoric dissolved organic matter (CDOM) and fluorescent dissolved organic matter (FDOM), and various key microbiological parameters, i.e. abundance, production, and respiration of marine heterotrophic prokaryotes.

## 2. Material and Methods

### 2.1. Seawater sampling and filtration

To carry out the BC-derived DOM biodegradation experiment, seawater was collected and filtered to prepare 1) natural DOM solutions (0.2-µm-filtered seawater), 2) BC-derived DOM stock solutions (made from mixing various BC materials with 0.2-µm-filtered seawater), and 3) the natural prokaryotic assemblage, i.e. concentrated bacterial inoculum (made from 0.8-µm-filtered seawater). Seawater was sampled at 5-m depth at the *Site d'Observation Littoral pour l'Environnement du MIO* (SOLEMIO) station (43.24°N, 5.29°E) located in the bay of Marseille (south of France) in the northwestern Mediterranean Sea (Fig. S1).

For the natural DOM solutions and BC-derived DOM stock solutions, 60 L of seawater was collected on board the R/V *Antédon 2* on May 5, 2021 (Fig. S2) using a pneumatically-operated Teflon ASTI pump. The seawater was pumped on board in Teflon tubing and then filtered in-line onto a pre-combusted 142-mm glass fiber filter (GF/F, Whatman®). The GF/F-filtered seawater was stored in three pre-cleaned 20-L polycarbonate (Nalgene®) bottles that were rinsed three times with seawater before filling. Back in the laboratory, this pumped and filtered seawater was transferred into 12 pre-combusted 5-L glass (Schott®) bottles (Fig. S2). DOC concentration of the GF/F-filtered seawater was 80 µM (Table S1).

Around 7 L of the GF/F-filtered seawater was used to prepare the BC-derived DOM stock solutions by immediately filtering at 0.2 µm through a Polycap TF PTFE capsule filter (0.2 µm, 1000 $cm^2$, Whatman®) assembled on a peristaltic pump line with silicon tubing for water circulation (Fig. S2). The filtration assembly was extensively rinsed with 20 L of ultrapure water (Milli-Q water, final resistivity: 18.2 MΩ cm), then rinsed with 1 L of GF/F-filtered seawater before collecting 6 L of 0.2-µm-filtered seawater into pre-combusted glass bottles. This 0.2-µm-filtered seawater, which had a DOC concentration of 82 µM (Table S1), was used to prepare BC-derived DOM stock solutions (Fig. S2) and was stored at 4°C in the dark before use (see section 2.2).

Around 53 L of the GF/F-filtered seawater was used to study natural DOM. This filtered seawater was kept in the laboratory in the 5-L glass bottles for around two weeks at 20°C in the dark to be slightly 'aged' to reduce the background levels of organic carbon in water (Nyholm and Kristensen, 1992; Wennberg et al., 2022). The bottles were opened and stirred at regular intervals. On 21 May 2021, ~40 L of this GF/F-filtered seawater was filtered at 0.2 µm through the Polycap TF PTFE capsule filter as described above, and the 0.2-µm-filtered seawater thus recovered was stored in pre-combusted 5-L glass bottles (Fig. S2). Subsampling was conducted for determinations of DOC and inorganic nutrient

concentrations. DOC concentration ranged from 70–75 µM. Silicate [$Si(OH)_4$] concentration ranged from 5.2–6.8 µM. Nitrate ($NO_3^-$), nitrite ($NO_2^-$), ammonium ($NH_4^+$) and phosphate ($PO_4^{3-}$) concentrations were very low (< 0.04 µM) (Table S1).

The remaining slightly aged GF/F filtered seawater (~13 L) was also filtered onto 0.2 µm (on May 25, 2021), but in sterile conditions under a low vacuum (< 50 mm Hg) with a 0.2-µm polycarbonate filter (47-mm diameter, Nuclepore), extensively rinsed with 10% hydrochloric acid (HCl), ultrapure water and seawater before use, mounted on a 47-mm polysulfone filtration system allowing the collection of the filtrate directly into a glass bottle. Sterile conditions were followed by autoclaving all the equipment (filtration system, glass bottles…) and working as much as possible under a laminar flow hood. The 0.2-µm filtered seawater retrieved was stored in three pre-combusted 2-L glass bottles (filled to 1.90 L) and used as natural DOM for the treatment without addition of the bacterial inoculum (Fig. S2). All bottles were stored at 20°C in the dark a few hours before being used to prepare the incubation solutions and the subsequent biodegradation experiment (see section 2.3).

For preparation of the concentrated bacterial inoculum, 12 L of seawater was collected on 31 May 2021 (Fig. S1, S2) with a GO-FLO bottle and stored in a pre-cleaned 20-L polycarbonate bottle. Back in the laboratory, 10 L of this seawater was filtered under low vacuum via a 47-mm glass filtration unit onto 0.8-µm and then 0.2-µm polycarbonate filters (Nuclepore) that had been extensively rinsed before use. The 0.2-µm filters containing the natural prokaryote assemblage were resuspended into 780 mL of 0.8-µm-filtered seawater stored in a pre-combusted 1-L glass bottle (Fig. S2). Cytometry measurements served to ensure a sufficient concentration of marine prokaryotes in the solution ($4.55.10^6$ cell $mL^{-1}$) to conduct the biodegradation experiment. DOC concentration in this solution was 88 µM (Table S1). The concentrated bacterial inoculum was stored for a few hours at 20°C in the dark

before being used to prepare the incubation solutions and for the subsequent biodegradation experiment (see section 2.3).

### 2.2. Preparation of the BC-derived DOM stock solutions

Three different BC-type materials were used for this biodegradation experiment. **1)** A Diesel Particulate Matter (DPM) standard reference material (NIST® SRM® 2975) purchased from Sigma-Aldrich, which is a standard reference for diesel exhaust particles (DEP) generated by diesel-powered industrial forklift and collected by a particular filtering system (Wright et al., 1991; Singh et al., 2004; Farahani et al., 2021), hereafter referred to as "$D_{REF}$". **2)** A DPM that had been oxidized before use, hereafter referred to as "$D_{REF\text{-}OX}$". For $D_{REF\text{-}OX}$, oxidation was performed by exposing DPM to an ultraviolet C (UVC) lamp (Pen-Ray® mercury discharge lamp; 185 nm, 1.38 W) (Saiz-Lopez et al., 2004; Bale et al., 2008) derived from a SOG-1 ozone generator (UVPA97, Analytik Jena). DPM (from 204 to 500 mg) was placed in the bottom of a 250-mL glass bottle, with the UVC lamp housed in its quartz tube placed above. The DPM was exposed to UVC for ~8 h. **3)** Soot collected in February 2021 in the chimney of a merchant ship (length: 140 m, width: 25 m, load capacity: 22,000 tons) running on heavy fuel oil (HFO) that was moored in Haiphong harbor, the leading seaport of northern Vietnam. This soot is hereafter referred to as "$D_{SHIP}$" (Fig. S2).

To obtain the desired DOC concentrations in the BC-derived DOM stock solutions, fairly large quantities of $D_{REF}$ and $D_{REF\text{-}OX}$ particles (which are strongly hydrophobic materials) were gradually added into the previously-prepared 0.2-µm-filtered seawater. Between 243 and 783 mg of $D_{REF}$ particles and between 204 et 500 mg of $D_{REF\text{-}OX}$ particles were then introduced into their respective 2-L glass bottles, and the solutions were placed in an ultrasonic bath for ~3 h to solubilize the particles. The solubilized solutions were then filtered onto a pre-combusted 47-mm GF/F filter. DOC concentration was measured on the

GF/F filtered solutions. The procedure (addition of particles, ultrasonic bath, filtration, DOC measurement) was repeated four times for $D_{REF}$ particles and three times for $D_{REF\text{-}OX}$ particles to reach the targeted DOC concentrations (see below). Overall, 2326 mg of $D_{REF}$ particles and 1287 mg of $D_{REF\text{-}OX}$ particles were introduced into 1 L of 0.2-µm-filtered seawater (Fig. S3). $D_{SHIP}$ particles, which were much more water-soluble than $D_{REF}$ and $D_{REF\text{-}OX}$ particles, were introduced at once (713 mg) (Fig. S3). The three GF/F-filtered solutions were finally filtered at 0.2 µm to provide the 1-L BC-derived DOM stock solutions of the three materials ($D_{REF}$, $D_{REF\text{-}OX}$, $D_{SHIP}$). These stock solutions were prepared on 18 May 2021 (Fig. S2).

In these BC-derived DOM stock solutions, the DOC concentrations related to addition of BC were 1763, 2276 and 3938 µM for the $D_{REF}$, $D_{REF\text{-}OX}$ and $D_{SHIP}$ materials, respectively. The concentrations of inorganic nutrients in these three solutions are reported in Table S1. The solutions were stored for a few hours at 20°C in the dark before being used to prepare the incubation solutions and for the subsequent biodegradation experiment (see section 2.3).

### 2.3. Preparation of the incubation solutions and biodegradation experiment

Five treatments were prepared and incubated for 90 days in triplicate (giving 15 incubation bottles): four biotic conditions (with presence of the bacterial inoculum) and one "abiotic" condition (without the bacterial inoculum). The four biotic conditions were $D_{REF}$, $D_{REF\text{-}OX}$ and $D_{SHIP}$ treatments (= natural DOM solution + BC-derived DOM stock solution from $D_{REF}$, $D_{REF\text{-}OX}$ or $D_{SHIP}$ + bacterial inoculum), and a control treatment ("C") without added BC-derived DOM (= natural DOM solution + bacterial inoculum) (Fig. S2). The abiotic condition was $D_{SHIP\text{-}Ab}$: $D_{SHIP}$ treatment without the bacterial inoculum (= natural DOM solution + BC-derived DOM stock solution from $D_{SHIP}$).

The incubation solutions were prepared on 1 June 2021 in the pre-combusted 5-L glass bottles (for C, $D_{REF}$, $D_{REF\text{-}OX}$ and $D_{SHIP}$ treatments) or 2-L glass bottles (for $D_{SHIP\text{-}Ab}$ treatment)

containing the natural marine DOM at volumes of 2900–3270 mL (for C, $D_{REF}$, $D_{REF\text{-}OX}$, $D_{SHIP}$) or 1900 mL (for $D_{SHIP\text{-}Ab}$) (Table 1). The BC-derived DOM stock solutions were added at volumes of 100–370 mL. Then, 60 mL of the concentrated bacterial inoculum solution was added to each incubation bottle for C, $D_{REF}$, $D_{REF\text{-}OX}$ and $D_{SHIP}$ treatments, and stock solutions of $NO_3^-$ and $PO_4^{3-}$ were added at volumes of 0–1 mL. The final overall volumes of incubation solution were ~3330 mL for C, $D_{REF}$, $D_{REF\text{-}OX}$ and $D_{SHIP}$ treatments, and 2000 mL for $D_{SHIP\text{-}Ab}$ (Fig. S2; Table 1). The incubation bottles were shaken gently for a few minutes to thoroughly mix the solutions.

We thus obtained final concentrations of ~200 µM BC-derived DOC and ~270 µM total DOC (i.e. BC-derived DOC + natural DOM-derived DOC + bacterial inoculum-derived DOC) for the $D_{REF}$, $D_{REF\text{-}OX}$ and $D_{SHIP}$ treatments and 73 µM DOC for the C treatment. These final concentrations of 200 µM BC-derived DOC in the incubation solutions were in line with DOC concentrations measured in coastal marine waters strongly impacted by atmospheric and riverine inputs of BC, i.e. up to 133 µM DOC in surface water and up to 279 µM DOC in the surface microlayer of Halong Bay, Vietnam (Mari et al., 2017). $NO_3^-$ and $PO_4^{3-}$ were added in the incubation solutions to avoid inorganic nutrient limitation during the 90-day biodegradation experiment. The theoretical final concentrations of DOC and dissolved inorganic nutrients in the incubation solutions are reported in Table S2.

Once the incubation solutions were well-mixed, the first sampling point was performed (T0; on 1 June 2021), after which the C, $D_{REF}$, $D_{REF\text{-}OX}$ and $D_{SHIP}$ solutions (in 5-L bottles) were transferred into 2.5-L pre-combusted amber glass bottles. Incubation was carried out for 90 days in the dark in a thermostatic room at 20°C, with the 15 bottles opened and shaken at regular intervals. Sampling points were performed on the 1$^{st}$ (T1), 2$^{nd}$ (T2), 3$^{rd}$ (T3), 7$^{th}$ (T4), 30$^{th}$ (T5) and 90$^{th}$ day (T6; on 31 August 2021) to determine the key chemical and microbiological parameters (Tables S3, S4). One part of this sampled water was immediately

filtered under a low vacuum onto GF/F filters for subsequent analyzes of DOC, dissolved organic nitrogen (DON), dissolved organic phosphorous (DOP), CDOM and FDOM, DBC, dissolved PAHs (d-PAHs), and dissolved inorganic nutrients (NUT), or onto pre-cleaned 0.2-µm polyesthersulfone syringe filters (SUPOR Acrodisc) in an ISO-5-class cleanroom for subsequent analyzes of dissolved trace elements (d-TM). Aliquots were also sampled without filtration for subsequent analyzes/measurements of bacterial abundance (BA), production (BP), respiration (BR) and abundance of heterotrophic nanoflagellates (Tables S3, S4).

### 2.4. Analyzes

***2.4.1. Dissolved organic carbon (DOC).*** GF/F-filtered samples were transferred into 20-mL pre-combusted glass vials with clean Teflon-lined caps and acidified with 20 µL of sulfuric acid ($H_2SO_4$; 95%, Sigma Aldrich). The vials were stored a few days at 4°C in the dark before analysis. DOC concentrations were determined by high-temperature platinum (Pt)-catalyzed oxidation coupled to non-dispersive infrared gas detection of carbon dioxide ($CO_2$) using a Shimadzu TOC-V carbon analyzer as per Sohrin and Sempéré (2005) and Fourrier et al. (2022). Before injection, the samples were bubbled for 2 min with $CO_2$-free air to purge inorganic carbon. The accuracy of the instrument and the system blank were determined by analysis of certified water references (batch 10-19, Hansell Laboratory). The nominal precision of the analysis procedure was within 2%.

***2.4.2. Chromophoric dissolved organic matter (CDOM).*** GF/F-filtered samples were transferred into 20-mL pre-combusted glass vials with clean Teflon-lined caps and stored at 4 °C until analysis. For the analyzes, the samples were brought to room temperature (20°C) in the dark and then transferred into a 1-cm Suprasil quartz cuvette for absorbance measurements on a Shimadzu UV-Visible 2450 spectrophotometer (Ferretto et al., 2017; Tedetti et al., 2020). Absorbance spectra were generated in single beam mode at between 200

and 800 nm with a wavelength interval of 1 nm, a slit width of 1 nm, and a scan speed of 230 nm $min^{-1}$. Between each analysis, the cuvette was successively rinsed with ultrapure water, methanol, ultrapure water, and finally the sample. The precision of the absorbance measurements was > 97% over the range 220–700 nm.

The absorbance values were corrected for blank and baseline drift, and then converted into CDOM absorption coefficients [$a_{CDOM}(\lambda)$ in $m^{-1}$] (Ferretto et al., 2017). The spectral slope coefficients between 275 and 295 nm ($S_{275-295}$ in $nm^{-1}$) and between 350 and 400 nm ($S_{350-400}$ in $nm^{-1}$) and the slope ratio (Sr: $S_{275-295}/S_{350-400}$) were determined as per Helms et al. (2008). The specific UV absorbance at 254 nm ($SUVA_{254}$, in L mg $C^{-1}$ $m^{-1}$) was calculated as $a_{CDOM}(254)$ divided by DOC concentration (in mg C $L^{-1}$), as per Weishaar et al. (2003).

***2.4.3. Fluorescent dissolved organic matter (FDOM).*** Sample storage conditions were the same as for CDOM measurements. For the analyzes, the samples were brought to 20°C in the dark and then transferred into a 1-cm Suprasil quartz cuvette for fluorescence measurements using a Hitachi F-7000 spectrofluorometer. Excitation-emission matrices (EEMs) were generated over an excitation wavelength ($\lambda_{Ex}$) range of 200–500 nm at 5-nm intervals and an emission wavelength ($\lambda_{Em}$) range of 280–550 nm at 2-nm intervals, a scan speed of 1200 nm $min^{-1}$, slit widths of 5 nm, and a PMT voltage of 700 V (Tedetti et al., 2012, 2016; Martias et al., 2018). The cuvette was rinsed between each sample as for CDOM.

The EEMs were normalized to the water Raman scatter peak, corrected for inner filtering effects using absorption measurements and Ohno (2002)'s formula, blank-corrected by subtracting the ultrapure water EEMs, and converted into quinine sulfate units (QSU) (Coble, 1996; Murphy et al., 2008). EEMs were then processed using parallel factor analysis (PARAFAC) in DOMFluor toolbox v1.6. running under MATLAB 9.11 (R2021b) as per Stedmon and Bro (2008). We also determined two fluorescence indices: humic index (HIX) (Zsolnay et al., 1999; Ohno, 2002), and biological index (BIX) (Huguet et al., 2009).

***2.4.4. Dissolved black carbon (DBC).*** DBC was analyzed as benzenepolycarboxylic acids (BPCAs) after nitric acid oxidation following the method of Dittmar (2008). GF/F-filtered samples were transferred into 500-mL pre-combusted glass (Schott®) bottles with clean Teflon-lined caps and stored at –20°C until analysis. After defrosting at room temperature, the samples were acidified to pH 2 with HCl, and then passed through a Bond-Elut PPL type cartridge (1 g, 6 mL, Agilent Technologies) at a flow rate of 3 mL $min^{-1}$ for solid-phase extraction (SPE) of DOM (Dittmar et al., 2008). The cartridge was then rinsed with 10 mL of acidified ultrapure water, dried under nitrogen stream, and finally eluted with 10 mL of methanol. The extracts were reduced in volume then introduced into 5-mL glass ampoules and evaporated to dryness. A volume of 0.5 mL of nitric acid ($HNO_3$; 70%, redistilled, Sigma) was added to the ampoules that were then sealed and placed in a DAB-3-250-mL stainless steel digestion reactor equipped with a 250-mL PTFE insert. Five mL of water were added to the insert so that the ampoules did not explode during the nitric-oxidation of the DOM. The reactor was then placed in an oven at 170°C for 6 h. The reactor was then left to cool back down to room temperature, then opened under an extractor hood. The ampoules were cooled for a few minutes at –18°C, then opened.

The oxidized extracts were taken up in a few hundred mL of methanol. An internal quantification standard, biphenyl-2,2'-dicarboxylic acid (BCA, Sigma), was then added (100 µL of a 10 µg $mL^{-1}$ solution in methanol) with the derivatization reagent, trimethylsilyl-diazomethane in hexane [$(CH_3)_3SiCHN_2$, Sigma], to produce methyl esters of BPCAs (Me-BPCAs) through a methyl esterification reaction (Ziolkowski et al., 2011; Zhong et al., 2019). Once the derivatization was complete, the samples were evaporated to dryness, taken up in 1 mL of dichloromethane ($CH_2Cl_2$), and injected into a Trace-ISQ GC ultra GC-MS system (ThermoElectron) equipped with a DB-5MS Ultra Inert column (Zhong et al., 2019).

The identification of Me-BPCAs was confirmed by the retention time and measurement of the compounds in selected ion monitoring (SIM) mode. The quantification was based on the response of the Me-BPCAs in relation to the response and amount of BCA internal standard introduced. Once the individual BPCA concentrations were determined, the DBC concentrations in the samples were estimated using the following formula (Dittmar, 2008; Stubbins et al., 2015; Yamashita et al., 2022):

$$[\mathrm{DBC}] = 33.4 \times ([\mathrm{B6CA}] + [\mathrm{B5CA}] + 0.5\,[\mathrm{B4CA}] + 0.5\,[\mathrm{B3CA}])$$

where [B3CA], [B4CA], [B5CA] and [B6CA] are the concentrations (in µM) of tricarboxylic, tetracarboxylic, pentacarboxylic and hexacarboxylic benzene acids, respectively, 33.4 is the average number of C atoms contained in a typical 7-ring DBC molecule, and [DBC] is the concentration of DBC in µM C. Here the DBC concentrations are reported in µg C $L^{-1}$.

For quality control and validation of the method, blanks were run, and during each digestion series, one ampoule out of the seven was used for the analysis of a reference organic matter (NOM 2R101N IHSS; Suwannee River Humic Acid Standard III 3S101H IHSS; Urban Dust 1649b) in order to check that the protocol was running correctly and to intercalibrate our results with previous studies (Dittmar, 2008; Ziolkowski et al., 2011; Nakane et al., 2017; Zhong et al., 2019).

***2.4.5. Dissolved polycyclic aromatic hydrocarbons (d-PAHs).*** We determined 19 parent PAHs and 15 groups of alkylated PAHs. The parent PAHs were: naphthalene (Nap), acenaphthylene (Acy), acenaphthene (Ace), fluorene (Fl), dibenzothiophene (DBT), phenanthrene (Phe), anthracene (Ant), fluoranthene (Flu), pyrene (Pyr), benz[a]anthracene (BaA), chrysene (Chr), benzo[b]fluoranthene (BbF), benzo[k]fluoranthene (BkF), benzo[e]pyrene (BeP), benzo[a]pyrene (BaP), perylene (Per), dibenz[a,h]anthracene (DahA), benzo[g,h,i]perylene (BghiP), and indeno[1,2,3-cd]pyrene (IcdP). The alkylated PAHs were the methyl-, dimethyl-, and trimethyl- homologs of Nap, Fl, Phe, Ant, Flt, Pyr, BaA and Chr.

Naphthalenes, fluorenes, dibenzothiophenes, and phenanthrenes/anthracenes correspond to the sum of parent and their alkylated derivatives. Samples were spiked with a mixture of deuterated standards (surrogates), i.e. Nap-$d_8$, Fl-$d_{10}$, Phe-$d_{10}$, Flu-$d_{10}$ and BaP-$d_{12}$, then extracted using liquid-liquid extraction with $CH_2Cl_2$ (2 × 60 mL per liter) as per the method developed by Guigue et al., 2015. These extracts were then concentrated using a rotary evaporator before changing the solvent to *n*-hexane. Hexane extracts were then purified to separate the hydrocarbon fraction from more polar compounds. Extracts were fractionated within a 500-mg silica column that had previously been activated at 500°C for 4 h then partially deactivated with ultrapure water (2% w/w). PAHs were eluted using 3 mL of *n*-hexane/$CH_2Cl_2$ (3:1 v/v). This was followed before analysis by a solvent reduction and the addition of a mixture of deuterated standards: Ace-$d_{10}$, Ant-$d_{10}$, Pyr-$d_{10}$, Chr-$d_{12}$ and Per-$d_{12}$.

PAHs were analyzed by GC-MS (Trace-ISQ GC ultra, ThermoElectron) operating at an ionization energy of 70 eV, with hydrogen (1.2 mL $min^{-1}$) as carrier gas. The capillary column (DB-5MS Ultra Inert, Agilent Technologies) was 30 m in length with an internal diameter of 0.25 mm and a film thickness of 0.25 μm. Injector (used in splitless mode) and detector temperatures were 250 and 320°C, respectively. PAHs were identified and quantified in full-scan and SIM mode simultaneously (Barhoumi et al., 2023).

The quality control procedures were strictly followed throughout the whole sampling and laboratory treatment process. They included control/validation of GC-MS calibration and tuning, blanks, limits of detection/quantification of the method (LODs/LOQs), and surrogate recoveries. Reference solutions for calibration (non-deuterated external standards), i.e. a mixture of 16 parent PAHs (04071, Fluka, 47543-U, Supelco, others from Sigma), were used to identify and quantify the compounds. LOQs ranged from 100–300 pg $L^{-1}$. Blank values were below LODs or LOQs. Surrogate recoveries were > 70%. Therefore, all the data reported here were neither blank-corrected nor recovery-corrected. The solvents (Rathburn

Chemicals Ltd, Scotland) were HPLC-grade. Standards and clean-up powder (Merck, Sigma Aldrich, France) were of ≥ 98% purity and high-purity grade, respectively.

***2.4.6. Other analyzes.*** A description of the analytical methods for dissolved inorganic nutrient, DON, DOP and dissolved metal trace elements is provided in the supplementary material (Text S1, S2, S3).

***2.4.7. Abundances of heterotrophic prokaryotes.*** To measure the abundances of heterotrophic prokaryotes (hereafter abbreviated 'BA' for bacterial abundances), samples (1.8 mL) were fixed with 18 µL of a preservative solution (glutaraldehyde, 0.25% final–pluronic acid, 0.01% final), kept for 15 min at room temperature in the dark, and then stored at –80°C until to enumeration of heterotrophic prokaryotes (HP) by flow cytometry. After thawing, samples were stained with SYBR Green (1X final concentration) for 15 min in the dark, and the HP were counted with an Accuri C6 flow cytometer (BD Biosciences). Fifty µL of sample were run at a flow rate of 35 µL $min^{-1}$. Non-fluorescent polystyrene microspheres (Flow Cytometry Size Calibration Kit, Thermo Fisher Scientific) were used as a size standard. Particles considered as HP were smaller than 2.0 µm, exhibited low complexity (low side scattering), emitted green fluorescence and no red fluorescence (Grégori et al., 2001). Data was acquired using BD Accuri CFlow Plus software. BA was expressed as cells per milliliter (cell $mL^{-1}$).

***2.4.8. Abundance of heterotrophic nanoflagellates***. At collection, 1980 µL of sample was fixed with 20 µL glutaraldehyde containing pluronic acid, and frozen at –80°C prior to analysis. At analysis, 25 µL of Trucount™ counting beads (BDBiosciences - batch of 49050 beads/tubes in 0.5 mL of sheathing fluid/pluronic acid) and 15 µL of 2-µm-diameter Fluoresbrite™ reference beads (Polysciences) were added to 1200 µL of thawed sample. Analyzes were performed on a CytoFlex flow cytometer (Beckman Coulter) of the PRECYM flow cytometry platform (https://precym.mio.osupytheas.fr/) (acquisition volume: 1000 µL,

acquisition speed: 120 µL $min^{-1}$) using green fluorescence (collected using a 530/30BP filter) to discriminate heterotrophic cells and eliminate non-heterotrophic cells. Data were acquired and analyzed using Beckman Coulter CytExpert 2.3 software.

***2.4.9. Heterotrophic prokaryotic production.*** Heterotrophic prokaryotic production (hereafter abbreviated 'BP' for bacterial production) was estimated from rates of protein synthesis with $^{3}$H-leucine incorporation using the microcentrifugation technique (Smith and Azam, 1992) as detailed in Van Wambeke et al. (2020). Briefly, subsamples of 1.5 mL were incubated in the dark at 20°C for between 0.3 and 2 h according to expected activities. Leucine was added at 20 nM (final concentration, using a mix of cold and radioactive leucine (specific activity: 100 Ci $mole^{-1}$). Linearity of leucine incorporation with time and isotopic dilution were checked periodically using time-series and concentration kinetics. The leucine-to-carbon conversion factor used was 1.5 kg C $mol^{-1}$.

***2.4.10. Bacterial respiration (BR).*** Samples were transferred into 1-mL volume Winkler vials in which dissolved oxygen ($O_2$) concentration was measured continuously by oxygen microprobes. The microprobes (Unisense, Denmark) are designed with an external guard cathode (Revsbech, 1989) resulting in extremely low $O_2$ consumption by the electrodes themselves (4.7 to $47\times10^{-7}$ mmol $O_2$ $h^{-1}$). The probes have a response time of less than 1 s and an accuracy of 0.1 µM. $O_2$ concentration was measured at regular time-intervals over a period of 24 h. Each measurement point corresponds to the continuous computer-recorded acquisition by the probes at 1 Hz for 60 s. BR was then determined from the slope of $O_2$ *vs.* time measured for a period of 3 to 5 h, which we assumed to be short enough to minimize changes in BA or BP in the Winkler vials. The starting point for slope calculation was defined based on the observed significant decrease in $O_2$ (0.5 µM) over incubation time. $O_2$ consumption was converted into BR (in µg C $L^{-1}$ $h^{-1}$) assuming a respiratory quotient of 1.

## 3. Results

### 3.1. Content of BC-derived DOM solutions at T0

Differences emerged between controls and the 4 BC treatments ($D_{REF}$, $D_{REF\text{-}OX}$, $D_{SHIP}$, $D_{SHIP\text{-}Ab}$), highlighting the impact of the soot addition and soot type on the composition of BC-derived DOM solutions. At T0, the DOC concentrations, which were proportional to the soot amount introduced in seawater (Fig. S3), were significantly higher in BC treatments (mean: 244–266 µM) than in C (mean: 74 µM) (t-test, $p < 0.05$), albeit slightly lower in $D_{REF\text{-}OX}$ (mean: 244 µM) than in $D_{REF}$ and $D_{SHIP}$/$D_{SHIP\text{-}Ab}$ (mean: 265 µM) (t-test, $p < 0.05$) (Table 2). DON concentrations were higher in the 4 BC treatments (mean: 8–12 µM) than in C (mean 3 µM) (t-test, $p < 0.05$), with the highest values in $D_{SHIP}$/$D_{SHIP\text{-}Ab}$ (mean: 12 µM) (t-test, $p < 0.05$). Conversely, DOP concentrations did not show any enrichment in the BC treatments relative to C (mean: < 0.2 µM) (Table 2).

DBC concentrations were significantly higher in the 4 BC treatments (mean: 869–974 µg C $L^{-1}$) than in C (mean: 12 µg C $L^{-1}$) (Table 2) (t-test, $p < 0.05$), and DBC/DOC ratios were also higher in the 4 BC treatments (mean: 30–31%) than in C (mean: 1%) (t-test, $p < 0.05$). In the five treatments, more than 60% of the measured BPCAs corresponded to BPCAs with 3 and 4 carboxyl groups (B3CA, B4CA), whereas BPCAs with 5 and 6 carboxyl groups (B5CA, B6CA) only accounted for 28% of the total DBC concentration in $D_{REF}$ and $D_{REF\text{-}OX}$ and 18% in $D_{SHIP}$ and $D_{SHIP\text{-}Ab}$ (Fig. 1). d-PAH concentrations were a little higher in $D_{REF\text{-}OX}$ (mean: 23–27 ng $L^{-1}$) than in C (mean: 14 ng $L^{-1}$) (t-test, $p < 0.05$) but were a whole order of magnitude higher in $D_{SHIP}$ and $D_{SHIP\text{-}Ab}$ (mean: 258-309 ng $L^{-1}$) (Table 2). In addition, the molecular composition of d-PAHs in $D_{SHIP}$ and $D_{SHIP\text{-}Ab}$, which showed a dominance of dibenzothiophenes (representing 80% of total d-PAHs), was markedly different from that of $D_{REF}$ and $D_{REF\text{-}OX}$ (Fig. 2). Naphthalenes and dibenzothiophenes appeared to be the major compounds in $D_{REF}$ (31 and 36% of total d-PAHs, respectively), whereas $D_{REF\text{-}OX}$ was

characterized by a dominance of phenanthrenes (34%), naphthalenes (21%) and benzoanthracene + chrysene (16%) and a very low dibenzothiophene content (~3%) (Fig. 2).

Although d-TM concentrations were not significantly different in the 5 treatments (mean: 30–36 µg $L^{-1}$) (Table 2), the relative abundance of individual metallic compounds showed a clear effect of the added soot. The 4 BC treatments were enriched in Zn relative to C (particularly $D_{REF}$ and $D_{REF\text{-}OX}$ where Zn accounted for 65% of total d-TM) and $D_{SHIP}$ and $D_{SHIP\text{-}Ab}$ were enriched in Fe (20% of total d-TM) compared to the other treatments (Fig. S4a) (t-test, $p < 0.05$). Nutrient concentrations (after adding $NO_3^-$ and $PO_4^{3-}$ to prevent limitation; Table 1) did not differ between the 4 BC treatments (except for $Si(OH)_4$ and $NO_2^-$ which were higher in $D_{REF}$, and $Si(OH)_4$) which was lower in $D_{SHIP\text{-}Ab}$) and were grossly similar to C (except for $NO_2^-$ and $NH_4^+$ which were lower in C) (Table 2).

Finally, the CDOM/FDOM indices calculated at the beginning of the experiment showed that the 4 BC treatments were enriched in chromophoric and fluorescent materials showing a very high degree of humification (HIX > 30), a low biological index (BIX < 1), and a high degree of aromaticity ($SUVA_{254}$ > 10 L mg $C^{-1}$ $m^{-1}$; $a_{CDOM}(254)$ > 30 $m^{-1}$) (Table 2). HIX (49), $SUVA_{254}$ (19 L mg $C^{-1}$ $m^{-1}$) and $a_{CDOM}(254)$ (60 $m^{-1}$) were highest in $D_{SHIP}$/ $D_{SHIP\text{-}ab}$ whereas HIX and $SUVA_{254}$ values were lower in $D_{REF\text{-}OX}$ (35 and 12 L mg $C^{-1}$ $m^{-1}$, respectively) compared to $D_{REF}$ (41 and 14 L mg $C^{-1}$ $m^{-1}$, respectively) (t-test, $p < 0.05$) (Table 2). These differences in content of the BC-derived DOM solutions in the 5 treatments at the start of the experiment influenced the biodegradation of the material by marine heterotrophic prokaryotes and the associated response of these organisms (see below).

### 3.2. Time-course of DOC, DBC and d-PAHs during biodegradation

Over the course of the experiment (from T0 to T6), DOC concentrations decreased significantly (t-test, $p < 0.05$) in $D_{REF}$ (by 20%), $D_{REF\text{-}OX}$ (by 21%), and $D_{SHIP}$ (by 9%), but did

not decrease significantly in C and $D_{SHIP\text{-}Ab}$ (Fig. S5). The strongest decreases were observed between T1 and T2 (between 1 and 2 days of incubation) (Fig. S5), which corresponded to bacterial exponential growth phase period (see section 3.6).

From T0 to T6, DBC concentrations decreased significantly (t-test, $p < 0.05$) in $D_{REF}$ (by 38%), $D_{REF\text{-}OX}$ (by 31%) and $D_{SHIP}$ (by 22%), but did not decrease significantly in $D_{SHIP\text{-}Ab}$ and remained stable in C (Fig. 3a). Data on the relative abundance of BPCAs showed that the proportion of B5CA + B6CA (relative to total BPCAs) increased significantly between the beginning (19%) and end (26%) of incubation in $D_{SHIP}$ (t-test, $p < 0.05$) while it remained stable in $D_{SHIP\text{-}Ab}$ (19%) (Fig. 1) and remained unchanged in $D_{REF\text{-}OX}$. A different trend was observed in the $D_{REF}$, which exhibited a slightly lower proportion of B5CA + B6CA at the end of incubation (24%) than at the beginning (27%).

d-PAH concentrations decreased between T0 and T6 by 55–64% in C, $D_{REF}$ and $D_{REF\text{-}OX}$ (t-test, $p < 0.05$ or 0.1). In $D_{SHIP}$, the decrease of 24% was non-significant because of the differences in triplicates (t-test, $p = 0.2$), while the d-PAH concentrations remained stable in $D_{SHIP\text{-}Ab}$ (Fig. 3b). In the biotic treatments, the decreases concerned mainly LMW d-PAHs (phenanthrenes, naphthalenes), while the concentrations of HMW d-PAHs (fluoranthene, pyrene) remained more stable after 3 months of incubation (Fig. 2; Table S7).

### 3.3. Identification and time-course of FDOM fluorophores

The PARAFAC model identified 5 FDOM components (C1-C5) validated on 105 samples collected throughout the biodegradation experiment for the different BC treatments (Fig. S6). Two classes of fluorophores were distinguishable. First, C1 and C4, with maxima at $\lambda_{Ex}/\lambda_{Em}$ of 245, 295/375 nm and 235, 290/356 nm, respectively, joining the class of protein-like fluorophores, with C4 associated with the T peaks and C1 close to peak N (Aiken, 2014; Coble et al., 2014). Second, C2, C3 and C5, which belonged to the humic-like fluorophore

class, with C5 ($\lambda_{Ex}/\lambda_{Em}$ of 260, 320/404 nm) related to peaks A + M, C2 ($\lambda_{Ex}/\lambda_{Em}$ of 230, 305/432 nm) related to peaks A + M/C, and C3 ($\lambda_{Ex}/\lambda_{Em}$ of 235, 365/484 nm) related to peaks A + C (Aiken, 2014; Coble et al., 2014) (Fig. S6).

The following text exclusively discusses the evolution of the C2 fluorophore, which was not detected in C. This particular fluorophore is widely regarded as the most representative one among the BC-derived DOM. At T0, the fluorescence intensities of C2 were maximal (6.5 QSU), minimal (1.4 QSU) and intermediate (2.6 QSU) in $D_{SHIP}$, $D_{REF\text{-}OX}$ and $D_{REF}$, respectively (Fig. 4; $D_{SHIP\text{-}Ab}$ not shown). The fluorescence intensity of C2 significantly decreased from T0 to T6 in all BC treatments (t-test, $p < 0.05$). In contrast, the fluorescence intensity in C remained consistently low throughout, without any significant changes. This decrease was most marked during the first 3 days of incubation (T3), after which C2 fluorescence intensity gradually decreased until stabilizing at the end of the experiment, resulting in an overall decrease from T0 to T6 of 83% in $D_{REF}$, 76% in $D_{SHIP}$, and 47% in $D_{REF\text{-}OX}$ (Fig. 4). This decrease in C2 fluorescence intensity was correlated to the decrease in DOC concentration, as seen in the observed significant positive linear correlation between the two parameters all times over the course of the experiment (from T0 to T6) and the three BC treatments (D, $D_{REF\text{-}OX}$, $D_{SHIP}$) combined ($R^2 = 0.66$, $n = 63$, $p < 0.05$) (Fig. S7).

### 3.4. Time-course of d-TM

Six trace metal elements measured at T0, T3 and T6 were selected to describe the dynamics of d-TM throughout the biodegradation process (Fig. S8; $D_{SHIP\text{-}Ab}$ not shown). Cu showed a significant and gradual increase over the course of the experiment. In the $D_{REF\text{-}OX}$ treatment, final Cu concentration was more than 3-fold higher than the initial concentration (0.32 µg $L^{-1}$ at T0 and 1.08 µg $L^{-1}$ at T6). Zn showed a non-significant decrease during biodegradation in $D_{REF}$ and $D_{REF\text{-}OX}$ but increased significantly in C and $D_{SHIP}$ (t-test, $p < 0.05$). Fe concentrations were relatively stable over time in C, $D_{REF}$ and $D_{REF\text{-}OX}$ but increased

very strongly in $D_{SHIP}$ (~65%). Pb concentrations remained relatively unchanged in C but decreased significantly in the three BC treatments (Fig. S8).

### 3.5. Time-course of nutrients, DON and DOP

DON and DOP concentrations remained stable over time (Fig. S9a, b; $D_{SHIP\text{-}Ab}$ not shown). $NO_2^-$ increased slightly between T3 and T6 in $D_{REF\text{-}OX}$ and $D_{SHIP}$ (11.8 and 32.6%, respectively) but showed no significant variation over time in $D_{REF}$ (Fig. S10a; $D_{SHIP\text{-}Ab}$ not shown). $NH_4^+$ concentrations did not show any significant variation over time in C. $NH_4^+$ concentrations decreased by 11% between T3 and T6 in in $D_{REF}$. $NH_4^+$ concentrations decreased significantly between T0 and T3 in $D_{REF\text{-}OX}$ (by 43%) and $D_{SHIP}$ (14%) but then increased significantly between T3 and T6 (by 49 and 43%, respectively) (t-test, $p < 0.05$) (Fig. S10b). $Si(OH)_4$ increased significantly over time in all treatments (t-test, $p<0.05$), while $NO_3^-$ and $PO_4^{3-}$ remained stable (not shown in the figures).

### 3.6. Dynamics of heterotrophic prokaryotes and nanoflagellates

For the three BC treatments $D_{REF,}$ $D_{REF\text{-}OX}$ and $D_{SHIP}$, bacterial abundance and production (BA and BP) presented a lag phase (BA) or a slight increase (BP) between T0 and T1 and a clearer increase between T1 and T2 (BP) or between T1 and T3 (BA), but then stabilized (Fig. 5a; Fig. 6a). BP decreased from T3 to the end of incubation (T6) whereas BA increased from T4 to T5 (Fig. 5a; Fig. 6a). This stabilization phase at T3 for BA and BP was also associated with a strong increase in the abundance of heterotrophic nanoflagellates, which then decreased gradually until the end of the incubation period (Fig. S11). C treatment showed a different pattern, with a less pronounced exponential phase reaching lower plateau values of BA and BP than in $D_{REF,}$ $D_{REF\text{-}OX}$ and $D_{SHIP}$ before a much more gradual decrease in BA and BP from T3 to T6 (Fig. 5a; Fig. 6a). In this condition, the abundance of heterotrophic

nanoflagellates, which was close to 0, showed no significant change over time (Fig. S11). Despite similar patterns in BA and BP between the 3 BC treatments, there were significant differences in the peak values of BA and BP and in the magnitude of BA and BP increase around T3. Regarding BA, $D_{REF}$ and $D_{SHIP}$ did not show any significant differences at T3, reaching 1.04 $10^6$ and 1.06 $10^6$ cell $mL^{-1}$, respectively, whereas $D_{REF\text{-}OX}$ showed a significantly higher BA of 1.64 $10^6$ cell $mL^{-1}$ at T3 (t-test, $p < 0.05$) (Fig. 5a). BP also showed significant differences between treatments and over time (t-test, $p < 0.05$). BP evolved in the same way in $D_{REF}$ and $D_{REF\text{-}OX}$ during the first day of the experiment but then it reached a peak of 1.4 $10^3$ ng C $L^{-1}$ $h^{-1}$ in $D_{REF\text{-}OX}$ at T3 compared to 6.49 $10^2$ and 8.99 $10^2$ ng C $L^{-1}$ $h^{-1}$ at T2 for $D_{SHIP}$ and $D_{REF}$, respectively (Fig. 6a). $D_{SHIP}$, again, afforded lower BP values than $D_{REF}$ and $D_{REF\text{-}OX}$ throughout the experiment.

Furthermore, during the growth-increase phase (~T1–T3), there was a negative power relationship between BP and bacterial respiration (BR) ($R^2 = 0.69$, $n = 36$, $p < 0.05$) (Fig. 7), which enabled us to define areas of dominant activity (BP *vs.* BR) for each treatment in the period between T0 and T3 corresponding to the exponential phase observed in all treatments. All the incubations presented two phases over time during the exponential phase: a first phase at T0–T1 characterized by a high BR (low BGE) and a second phase at T2–T3 associated with high BP (high BGE). In addition, the highest values for BR (6.4 ng $C^{-1}$ $L^{-1}$ $h^{-1}$) and BP (1447.6 ng $C^{-1}$ $L^{-1}$ $h^{-1}$) were observed in $D_{REF\text{-}OX}$, where most of the points measured were positioned at the extremes of the correlation. $D_{REF\text{-}OX}$ also shows the highest and lowest BGEs in the exponential phase, highlighting the occurrence of both activities performed at a higher intensity compared to the other treatments (Table S5). On the other hand, in $D_{REF}$, most of the points fell within a dominant production activity, with measured respiration values not exceeding 4 $10^4$ ng $C^{-1}$ $L^{-1}$ $h^{-1}$. $D_{SHIP}$ showed a particularly low BP at the beginning of the exponential phase (reaching a minimum of 22.7 ng $C^{-1}$ $L^{-1}$ $h^{-1}$), and the BP values measured in

this treatment were nearly always below 600 ng $C^{-1}$ $L^{-1}$ $h^{-1}$ (Fig. 7). When normalizing BA and BP to the DOC concentrations derived from the soot addition, fairly homogeneous BP values were obtained (Fig. 6b). However, the differences between DREF, DREF-OX, and DSHIP persisted for BA values (Fig. 5b).

The $D_{SHIP\text{-}Ab}$ treatment, which was intended to be abiotic, showed signs of biological activity, i.e. bacterial abundance and production, from T1 (1 day) (Fig. S12a, c), suggesting a contamination during the preparation of the incubation at T0. The dynamics of bacterial growth in $D_{SHIP\text{-}Ab}$ over time can be separated into two phases: a first phase (P1) from T0 to T3 (0 to 3 days) where bacterial abundance and production were significantly lower (t-test, $p < 0.05$) than in $D_{SHIP}$ treatment, and a second phase (P2) from T3 to T6 (3 days to 90 days) where $D_{SHIP\text{-}Ab}$ approaches $D_{SHIP}$ in terms of biological activity, without reaching such high values (Fig. S12a, c). In addition, the bacterial abundance and production normalized to DOC remained low in $D_{SHIP\text{-}Ab}$ compared to C and $D_{SHIP}$ (particularly for bacterial abundance) (Fig. S12b, d) (t-test, $p < 0.05$).

## 4. Discussion

### 4.1. Composition of BC-derived DOM in relation with the type of soot

Here we investigated the bioavailability of DOM derived from BC/soot of anthropogenic origin (combustion of fossil fuels), whereas most recent studies have focused more on the bioavailability of DOM derived from biomass-source BC (Qi et al., 2020; Bostick et al., 2021; Wagner et al., 2021; Goranov et al., 2022). The organic and inorganic content of BC-derived DOM solutions depends on the initial chemical composition of the soot particles that are added, but also on the solubility of these elements in seawater. The most hydrophobic fraction of the organic matter of the particles was most likely not transferred to

the aqueous phase during this experiment. However, the objective here was to simulate an input of soot to the ocean surface rather than to extract all the organic matter from the soot.

DPM reference material ($D_{REF}$) has been used as standardized DEP sample in numerous studies addressing the effects of fine particle air pollution on health (Delfino et al., 2009; Brook et al., 2010; Apte et al., 2018; Farahani et al., 2021) but also as a BC reference material to analyze BC in sediments (Elmquist et al., 2004; Im et al., 2008), to determine adsorption and partition components of organic compounds on BC (Chiou et al., 2015), and to observe microbial colonization of BC particles in coastal seawater (Benavides et al., 2019). To our knowledge, this is the first time that this DPM has served to produce DOM for a biodegradation experiment involving marine heterotrophic prokaryotes.

Apart from oxidized $D_{REF}$ ($D_{REF\text{-}OX}$), the other substrate used to assess the bioavailability of BC-derived DOM was soot collected in the chimney of a merchant ship running on HFO and moored in Haiphong harbor, Vietnam ($D_{SHIP}$). It is now recognized that maritime transportation and shipping activities are significant sources of particulate matter, pollutants and BC (Buffaloe et al., 2014; Huyen et al., 2022; Zhao et al., 2022). Recent studies have investigated the chemical composition of particles derived from HFO combustion by ships and their potential effects on human health (Popovicheva et al., 2009; Oeder et al., 2015; Corbin et al., 2018a, b), but to our knowledge, no work has addressed the effect of a ship's soot and its derived soluble fraction on marine heterotrophic prokaryotes.

Additions of the soluble fraction of soot to natural seawater ($D_{REF}$, $D_{REF\text{-}OX}$, $D_{SHIP}$/$D_{SHIP\text{-}Ab}$) led to strong enrichments of DOM in DOC, DON, DBC, d-PAHs, as well as CDOM and FDOM, and large increase in DBC/DOC ratio compared to the C treatment (Table 2). This is further evidence that particles emitted during combustion of diesel/HFO have contents of organic carbon, PAHs and BC (Popovicheva et al., 2009; Buffaloe et al., 2014; Corbin et al., 2018b; Farahani et al., 2021). Despite the DBC/DOC ratio being relatively consistent among

DREF, DREF-OX, and DSHIP (around 30%), we observed significant differences in other parameters.

$D_{REF}$ and $D_{REF\text{-}OX}$ brought low quantities of d-PAHs, increasing by only a factor ~ 2 the C value. The much greater supply of d-PAHs with a dominance of dibenzothiophenes (organosulfur compounds) in $D_{SHIP}$/$D_{SHIP\text{-}Ab}$ compared to $D_{REF}$ and $D_{REF\text{-}OX}$ (Table 2; Fig. 2) is in accordance with the high levels of PAHs and sulfur compounds, including benzothiophenes, detected in soot derived from HFO (Popovicheva et al., 2009; Corbin et al., 2018b; Zhao et al., 2022). The fact that the d-PAH pools in the three BC-derived DOM were dominated by LMW compounds (Table S7) is in good agreement with the lower hydrophobicity of these latter (Farahani et al., 2021). However, the d-PAH concentrations were overall very low with regard to the high amount of the added particles confirming the high hydrophobicity of the most of particle-bound compounds. Furthermore, despite near-identical DOC concentrations, CDOM and FDOM contents and the degrees of DOM humification (HIX) and aromaticity ($SUVA_{254}$) were much higher in $D_{SHIP}$/$D_{SHIP\text{-}Ab}$ than in $D_{REF}$ and $D_{REF\text{-}OX}$ (Table 2; Fig. S5). This could be due to a higher content in PAHs and other aromatic compounds in HFO particles ($D_{SHIP}$) compared to particles originating from lighter diesel fuels ($D_{REF}$) (Corbin et al., 2018b). Concerning d-TM, the main differences were the higher proportion of Zn in $D_{REF}$ and $D_{REF\text{-}OX}$ compared to $D_{SHIP}$/$D_{SHIP\text{-}Ab}$, and the higher proportion of Fe in $D_{SHIP}$/$D_{SHIP\text{-}Ab}$ compared to $D_{REF}$ and $D_{REF\text{-}OX}$ (Fig. S4a). Zn is more often associated with industrial activity than transport emissions (Li et al., 2017), and has previously been identified as one of the most abundant d-TM in DPM reference material, although its concentration has been found to be lower than in ambient particulate matter (PM) samples (Farahani et al., 2021). Fe, a known vehicle emissions tracer (Hulskotte et al., 2014; Charron et al., 2019), has been already reported as one of the dominant d-TM in HFO fuel and PM samples (Corbin et al., 2018a), which again is in line with our results.

Photooxidation of DPM (i.e. differences between $D_{REF}$ and $D_{REF\text{-}OX}$) did not show any significant effect on the proportion of DBC within DOC, nor on the proportion of BPCAs within the DBC pool (Table 2; Fig. 1). Similarly, there was no photooxidation effect on the composition of d-TM (Fig. S4a). However, photooxidation led to a decrease in the proportion of dibenzothiophenes within the d-PAH pool (Fig. 2). Note that photodegradation of PAHs bound to diesel/soot particles has already been reported (Matuzawa et al., 2001; Kim et al., 2013), although particulate PAHs appear to be less sensitive to photooxidation than dissolved PAHs in aqueous solution (Neff, 2002), and dibenzothiophenes have been shown to undergo degradation during photooxidation experiments (Liu et al., 2020). Finally, the net decrease in $SUVA_{254}$ and $a_{CDOM}(254)$ values from $D_{REF}$ to $D_{REF\text{-}OX}$ (Table 2) reflected the loss of chromophoric, aromatic and HMW dissolved material, along with structural modifications in the DOM linked to the oxidation (Ferretto et al., 2017).

The addition of soot and the subsequent BC-derived DOM solutions therefore significantly modified the chemical environment to which heterotrophic prokaryotes are receptive/sensitive, by behaving 1) as a more or less labile source of new DOM, and 2) as a source of nutrients and metals that can potentially impact BP. The nutrient concentrations measured here suggest that prokaryotes were not growth-limited and that the d-TM were not associated with major differences in BP or BR (Fig. S8, S9, S10). We thus considered that DOC and DBC lability were the main limiting factors influencing BP, BR, and time-course of DOC and DBC.

### 4.2. Bioavailability of BC-derived DOM and the microbial responses

The presence of BC-derived DOM led to a stimulation of bacterial activities (relative to the control) in the three BC treatments $D_{REF,}$ $D_{REF\text{-}OX}$ and $D_{SHIP}$. BA and BP increased significantly after a relatively short 24-h lag-phase. This stimulation, which corresponded to

the exponential phase of heterotrophic prokaryotic growth, was followed by periods of stabilization (stationary phase) and decrease (Fig. 5, 6), as well as an increase in heterotrophic nanoflagellates predators at T3 which was particularly evidenced in the experiments (Fig. S11). The short (24 h) lag phase suggested a near-immediate bioavailability of the BC-derived DOM (Lønborg and Álvarez-Salgado, 2012; Djaoudi et al., 2020). Furthermore, in the 3 BC treatments, the increase in BP and BR were associated with a consumption of BC-derived DOM, which was observed through the significant decreases of DOC, DBC and d-PAH concentrations from T0 to T6. These decreases provide argue that the BC-derived DOM was bioavailable. Although stimulations of BP and BR and consumption of BC-derived DOM were recorded in all the $D_{REF}$, $D_{REF\text{-}OX}$ and $D_{SHIP}$ treatments, the between-treatment differences could be linked to the chemical substrates present in each BC-derived DOM solution and/or to the composition/structure of the marine microbial community associated with each of these solutions.

The $D_{SHIP\text{-}Ab}$ treatment could not be considered as truly abiotic due to the presence of an active bacterial community (Fig. S12). Nevertheless, this bacterial community, particularly during P1, was much less abundant and much less active than those in the BC biotic treatments, and did not induce any significant decrease in DOC, DBC and d-PAH concentrations over the course of the experiment (Fig. S5, Table S6, 4). Hence, with the presence of a smaller bacterial community, the concentrations of DOC, DBC and d-PAHs remained quite stable from T0 to T6. Corollary, this showed that there was no significant effect of abiotic processes, such as sorption or flocculation, on DOC, DBC and d-PAH concentrations from T0 to T6. This thus tended to confirm our that the decrease in DOC, DBC and d-PAH concentrations recorded over time in $D_{REF}$, $D_{REF\text{-}OX}$ and $D_{SHIP}$ treatments was mainly due to marine prokaryotes and not to abiotic processes. This thus tended to confirm our that the decrease in DOC, DBC and d-PAH concentrations recorded over time in DREF,

DREF-OX and DSHIP treatments was mainly due to marine prokaryotes with a minor effect of abiotic processes. (Bostick et al., 2021; Goranov et al., 2022).

$D_{REF-OX}$ showed by far the highest peaks reached for abundances (BA), and activities (BP and BR) over the course of the biodegradation experiment, with the highest slopes in the exponential phases for BA and BP and the highest peak of BR reached during the first 72 h. These higher activities, especially for BR, were very likely related to the photooxidation of diesel particles and the subsequent occurrence of dissolved oxidized organic substrates in the BC-derived DOM solution, as these oxidized substrates are more easily and preferentially metabolized by bacteria (Crapart et al., 2021). These results are in line with a large number of studies demonstrating that pyrogenic carbon could support microbial respiration in soils (Fang et al., 2014; Kuzyakov et al., 2014; Khodadad et al., 2011; Zimmermann et al., 2012; Bamminger et al., 2014). The stimulation of BR at the beginning of biodegradation through the presence of oxidized substrates probably partly explains the fact that the BP levels were highest after 72 h of incubation, resulting finally in the highest BGE during the exponential phase. $D_{REF-OX}$ also showed the highest decreases in DOC and d-PAH concentrations between T0 and T6 (21 and 64%, respectively), which is consistent with the fact that it reached highest peaks of BP and BR, whereas it showed a slightly lower decrease in DBC concentration (31%) than $D_{REF}$ (38%). As mentioned previously, the photooxidation of the diesel material resulted in a significant reduction in the proportion of dibenzothiophenes, which are known to have toxic effects on bacteria (as discussed below).

The peak values of heterotrophic prokaryotic stocks (BA) and activities (BP and BR) were lower in the $D_{REF}$ treatment than in the $D_{REF-OX}$ treatment. Without the presence of photooxidized products, the metabolism of heterotrophic prokaryotes was shifted towards anabolism (BP), while the decreases in DOC and d-PAH concentrations between T0 and T6 in $D_{REF}$ (20 and 59%, respectively) were not far from the decreases recorded in $D_{REF-OX}$.

Interestingly, $D_{REF}$ showed the highest decrease in DBC concentration (38%) and was the only treatment that presented a significant decrease in B5CA + B6CA concentrations in addition to B3CA + B4CA concentrations (Fig. 1; Table S6) as well as a significant decrease in HMW PAHs (Table S7). This point suggests that in the absence of bioavailable oxidized compounds, the heterotrophic prokaryotic community was able to utilize the more condensed fraction of the organic material in addition to lighter/more labile molecules for biomass production.

$D_{SHIP}$ showed the lowest peaks in BA, BP and BR, as well as the lowest decrease in DOC (9%), DBC (22%) and d-PAHs (24%) throughout the experiment. This was probably related to the high abundance of dibenzothiophene (80% of total d-PAHs) found in this treatment. The high toxicity of this hydrocarbon almost certainly had a strong impact on the prokaryotic community (van Afferden et al., 1990; Li et al., 2019; Ghosh and Mukherji, 2021), but it appears that even under such treatments, there was still a significant decrease of DOM-BC and DBC concentrations over time. The significant decrease in the fluorescence of the C2 fluorophore (Fig. 4), which strongly correlated with DOC concentration (Fig. S7) but not with DBC concentration, points to a bioavailability of DBC itself in addition to the bioavailability of other compounds present in the BC-derived DOM pool.

Both the bulk DOC pool and its DBC fraction underwent biodegradation. The consumption of DBC, which was observed in all incubations through the decrease in BPCA concentrations (Fig. 3a; Table S6), highlights the bioavailability of the most aromatic and condensed moieties within the whole continuum of molecules brought by the solubilization of BC. In addition, the changes in composition of the measured BPCAs points to a variability in the efficiency of DBC degradation depending on the type of activity measured. These observations join up with Qi et al. (2020) and Goranov et al. (2022), who found that the

aromatic fraction of BC-derived DOM could be taken up and integrated into the biomass of heterotrophic prokaryotes.

## 5. Conclusion

This study, measuring significant decreases in DOC, PAH and DBC concentrations over time, reveals that bioavailability exists along the entire molecular continuum resulting from the solubilization of BC. The bioavailable fraction of DBC depends on two key factors: 1) the origin of the BC-soot material, which influences the composition, level of condensation, and oxidation of the matter released during its dissolution, and 2) the dynamics of the heterotrophic prokaryotic community in a controlled environment. Both factors contribute to a gradient of DBC bioavailability and also influence a shift in bacterial metabolism, favoring either anabolism or catabolism. Based on our findings, DBC recently introduced into marine waters from the deposition of fossil fuel combustion particles cannot be considered as belonging entirely to the refractory compartment of the DOM and thus associated with long-term oceanic storage. DBC should be also seen as a potentially more accessible material for marine prokaryotes, which could degrade it on a year-long scale in the ocean. It is now essential to further investigate the bioavailability of DBC originating from other sources (other types of fossil fuel combustion particles or biomass combustion particles), focusing particularly on its molecular composition and level of oxidation using FT-ICR-MS analyses, but also on the different prokaryotic assemblages and their ability to adapt to the use of this organic material.

A companion paper dedicated to bacterial diversity data from this biodegradation experiment is currently being prepared and is set to address the impact of DBC type on the arrangement and diversity of the marine heterotrophic prokaryotic community.

**Acknowledgments**

This work was conducted as part of 1) the BLACKMATTERS project (*Dissolved Black Carbon in marine waters: potential bioavailability for heterotrophic prokaryotes*) under the CONTAM (*CONTAMinants in marine ecosystems*) cross-disciplinary research area at the MIO laboratory, and funded by the IRD-Action Sud and MIO cross-disciplinary research programs, 2) the EU-MarTERA MATE project (*MAritime Traffic Emissions: A monitoring network*) funded by the Agence Nationale de la Recherche [French National Research Agency] (ANR-20-MART-0003), 3) the IRN SOOT-SEA (*International Research Network on the Impact of Black Carbon in South East Asia*), and 4) the LMI LOTUS (*International Joint Laboratory on the Land-Ocean-aTmosphere regional coUpled System*), both funded by the IRD. We thank the captains and crew of the R/V *Antédon 2* and *ASTROIDES*, as well as J.A. Tesán-Onrubia, L. Papillon, M. Lafont and D. Malengros for their excellent service at sea and invaluable assistance in collecting seawater samples. We also thank N. Garcia, P. Raimbault and the Plateforme Analytique de Chimie des Environnements Marins (PACEM platform) for their analyzes of inorganic nutrients, DON and DOP, as well as R. Freydier, L. Causse and the AETE-ISO platform at the OSU-OREME/Université de Montpellier for the trace metal analyzes. We thank M. Benavides and B. Misson (MIO) for their participation in thinking out and devising a scientific approach for this experiment and for their comments on the early version of the manuscript. P. Martinot holds a PhD scholarship provided by Aix-Marseille University on behalf of doctoral school 251 in environmental sciences (ED251, MENRT doctoral grant). Finally, we acknowledge two anonymous reviewers for their relevant comments and corrections.

**Supplementary information**

Supplementary material related to this article is available online at: xxxx

## References


Afferden, M.Y., Schacht, S., Klein J., Trüper, H.G., 1990. Degradation of dibenzothiophene by brevibacterium Sp.DO. Arch. Microbiol., 153(4), 324-28. https://doi.org/10.1007/BF00249000.

Aiken, G.R., 2014. Fluorescence and dissolved organic matter: A chemist's perspective. Aquatic organic matter fluorescence. Edited by P.G. Coble, J. Lead, A. Baker, D.M. Reynolds, R.G.M. Spencer. Cambridge Environmental Chemistry Series, Cambridge University Press, New York, NY, USA, pp. 35–75. ISBN: 9780521764612.

Aminot, A., Kérouel, R., 2004. Hydrologie des écosystèmes marins. Paramètres et analyses. Ed. Ifremer, 336 p.

Aminot, A., Kérouel, R., 2007. Dosage Automatique des Nutriments Dans Les Eaux Marines: Méthodes en Flux Continu. Edition Quae, Ifremer, Plouzané, France.

Andrew, A.A., Del Vecchio, R., Subramaniam, A., Blough, N.V., 2013. Chromophoric dissolved organic matter (CDOM) in the Equatorial Atlantic Ocean: Optical properties and their relation to CDOM structure and source. Mar. Chem., 148, 33-43. https://doi.org/10.1016/j.marchem.2012.11.001.

Apte, J. S., Brauer, M., Cohen, A. J., Ezzati, M., Pope III, C. A., 2018. Ambient PM2. 5 reduces global and regional life expectancy. Environ. Sci. Technol. Lett., 5(9), 546-551. https://doi.org/10.1021/acs.estlett.8b00360.

Bale, C.S.E., Ingham, T., Commane, R., Heard, D.E., Bloss, W.J., 2008. Novel measurements of atmospheric iodine species by resonance fluorescence. J. Atmos. Chem., 60, 51-70. https://doi.org/10.1007/s10874-008-9108-z.

Bamminger, C., Marschner, B., Jüschke, E., 2014. An incubation study on the stability and biological effects of pyrogenic and hydrothermal biochar in two soils. Eur. J. Soil Sci., 65(1), 72-82. https://doi.org/10.1111/ejss.12074.

Bao, H., Niggemann, J., Luo, L., Dittmar, T., Kao, S.-J., 2017. Aerosols as a source of dissolved black carbon to the ocean. Nat. Commun., 8. https://doi.org/10.1038/s41467-017-00437-3.

Barhoumi, B., Guigue C., Touil, S., Johnson-Restrepo, B., Driss, M.R., Tedetti, M., 2023. Hydrocarbons in the atmospheric gas phase of a coastal city in Tunisia: Levels, gas–particle partitioning, and health risk assessment. Sci. Total Environ., 879, 162986. http://dx.doi.org/10.1016/j.scitotenv.2023.162986.

Benavides, M., Chu Van, T., Mari, X., 2019. Amino acids promote black carbon aggregation and microbial colonization in coastal waters off Vietnam. Sci. Tot. Environ., 685, 527-532.

Bond, T.C., Doherty, S.J., Fahey, D.W., Forster, P.M., Berntsen, T., DeAngelo, B.J, Flanner, M.G., Ghan, S., Kärcher, B., Koch, D., Kinne, S., Kondo, Y., Quinn, P.K., Sarofim, M.C., Schultz, M.G., Schulz, M., Venkataraman, C., Zhang, H., Zhang, S., Bellouin, N., Guttikunda, S.K., Hopke, P.K., Jacobson, M.Z., Kaiser, J.W., Klimont, Z., Lohmann, U., Schwarz, J.P., Shindell, D., Storelvmo, T., Warren, S.G., Zender, C.S., 2013. Bounding the role of black carbon in the climate system: A scientific assessment. J. Geophys. Res. Atmos., 118, 5380-5552. https://doi.org/10.1002/jgrd.50171.

Bostick, K.W., Zimmerman, A.R., Goranov, A.I., Mitra, S., Hatcher, P.G., Wozniak, A.S., 2021. Biolability of fresh and photodegraded pyrogenic dissolved organic matter from laboratory-prepared chars. J. Geophys., 126, 1-17. https://doi.org/10.1029/2020JG005981.

Brook, R.D., Rajagopalan, S., Pope, C.A., Brook, J.R., Bhatnagar, A., Diez-Roux, A.V., Holguin, F., et al. 2010. Particulate Matter Air Pollution and Cardiovascular Disease: An Update to the Scientific Statement From the American Heart Association. Circ. J., 121(21): 2331-78. https://doi.org/10.1161/CIR.0b013e3181dbece1.

Buffaloe, G., Lack, D., Williams, E., Coffman, D., Hayden, K., Lerner, B. M., Li, S.-M., Nuaaman, I., Massoli, P., Onasch, T. B., Quinn, P. K., Cappa, C. D., 2014. Black carbon emissions from in-use ships: A California regional assessment. Atm. Chem. Phys. 14(4), 1881-1896. https://doi.org/10.5194/acp-14-1881-2014.

Céa, B., Lefèvre, D., Chirurgien, L., Raimbault, P., Garcia, N., Charrière, B., Grégori, G., Ghiglione, J.F., Barani, A., Lafont, M., Van Wambeke, F., 2015. An annual survey of bacterial production, respiration and ectoenzyme activity in coastal NW Mediterranean waters: temperature and resource controls. Environ. Sci. Pollut. Res., 22, 13654-13668. https://doi.org/10.1007/s11356-014-3500-9.

Charron, A., Polo-Rehn, L., Besombes, J.-L., Golly, B., Buisson, C., Chanut, H., Marchand, N., Guillaud, G., Jaffrezo, J.-L., 2019. Identification and Quantification of Particulate Tracers of Exhaust and Non-Exhaust Vehicle Emissions. Atm. Chem. Phys., 19(7): 5187-5207. https://doi.org/10.5194/acp-19-5187-2019.

Chiou, C.T., Cheng, J., Hung, W.-N., Chen, B., Lin, T.-F., 2015. Resolution of Adsorption and Partition Components of Organic Compounds on Black Carbons. Environ. Sci. Technol., 49, 9116-9123. https://doi.org/10.1021/acs.est.5b01292.

Coble, P.G., 1996. Characterization of marine and terrestrial DOM in seawater using excitation-emission matrix spectroscopy. Mar. Chem., 51, 325-346. https://doi.org/10.1016/0304-4203(95)00062-3.

Coble, P.G., Spencer, R.G.M., Baker, A., Reynolds, D.M., 2014. Aquatic organic matter fluorescence. In: Aquatic organic matter fluorescence. Edited by P.G. Coble, J. Lead, A. Baker, D.M. Reynolds, R.G.M. Spencer. Cambridge Environmental Chemistry Series, Cambridge University Press, New York, NY, USA, pp. 75-122. ISBN: 9780521764612.

Coppola, A.I., Druffel, E.R.M., 2016. Cycling of black carbon in the ocean. Geophys. Res. Lett., 43, 4477-4482. https://doi.org/10.1002/2016GL068574.

Coppola, A.I., Walker, B.D., Druffel, E.R.M., 2015. Solid phase extraction method for the study of black carbon cycling in dissolved organic carbon using radiocarbon. Mar. Chem., 177, 697-705. https://doi.org/10.1016/j.marchem.2015.10.010.

Coppola, A.I., Wiedemeier, D.B., Galy, V., Haghipour, N., Hanke, U.M., Nascimento, G.S., Usman, M., Blattmann, T.M., Reisser, M., Freymond, C.V., Zhao, M., Voss, B., Wacker, L., Schefuß, E., Peucker-Ehrenbrink, B., Abiven, S., Schmidt, M.W.I., Eglinton, T.I., 2018. Global-scale evidence for the refractory nature of riverine black carbon. Nat. Geosci., 11, 584-588.

Coppola, A.I., Wagner, S., Lennartz, S.T. Seidel, M., Ward, N.D., Dittmar, T., Santín, C., Jones, M.W., 2022. The black carbon cycle and its role in the Earth system. Nat. Rev. Earth Environ., 3(8), 516-532. https://doi.org/10.1038/s43017-022-00316-6.

Corbin, J.C., Mensah, A.A., Pieber, S.M., Orasche, J., Michalke, B., Zanatta, M., Czech, H., Massabò, D., Buatier de Mongeot, F., Mennucci, C., El Haddad, I., Kumar, N. K., Stengel, B., Huang, Y., Zimmermann, R., Prévôt, A. S. H., Gysel, M., 2018a. Trace metals in soot and PM2.5 from heavy-fuel-oil combustion in a marine engine. Environ. Sci. Technol., 52(11), 6714-6722. https://doi.org/10.1021/acs.est.8b01764

Corbin, J. C., Pieber, S. M., Czech, H., Zanatta, M., Jakobi, G., Massabò, D., Orasche, J., El Haddad, I., Mensah, A. A., Stengel, B., Drinovec, L., Mocnik, G., Zimmermann, R., Prévôt, A. S. H., Gysel, M., 2018b. Brown and black carbon emitted by a marine engine operated on heavy fuel oil and distillate fuels: Optical properties, size distributions, and emission factors. J. Geophys. Atmos., 123, 6175–6195. https://doi.org/10.1029/2017JD027818

Crapart, Camille, Tom Andersen, Dag Olav Hessen, Nicolas Valiente, Rolf David Vogt. 2021. Factors Governing Biodegradability of Dissolved Natural Organic Matter in Lake Water. Water, 13(16): 2210. https://doi.org/10.3390/w13162210.

Delfino, R.J., Staimer, N., Tjoa, T., Gillen, D.L., Polidori, A., Arhami, M., Kleinman, M.T., D. Vaziri, N.D., Longhurst, J., Sioutas, C., 2009. Air pollution exposures and circulating biomarkers of effect in a susceptible population: Clues to potential causal component mixtures and mechanisms. Environ. Health Persp. 117(8): 1232-38. https://doi.org/10.1289/ehp.0800194.

Dittmar, T., Koch, B., Hertkorn, N., Kattner, G., 2008. A simple and efficient method for the solid-phase extraction of dissolved organic matter (SPE-DOM) from seawater. Limnol. Oceanogr. Methods, 6, 230-235. https://doi.org/10.4319/lom.2008.6.230.

Dittmar, T., 2008. The molecular level determination of black carbon in marine dissolved organic matter. Org. Geochem., 39, 396–407. https://doi.org/10.1016/j.orggeochem.2008.01.015.

Dittmar, T., Koch, B.P., 2006. Thermogenic organic matter dissolved in the abyssal ocean. Mar. Chem., 102, 208–217. https://doi.org/10.1016/j.marchem.2006.04.003.

Dittmar, T., Paeng, J., 2009. A heat-induced molecular signature in marine dissolved organic matter. Nat. Geosci., 2, 175–179. https://doi.org/10.1038/ngeo440.

Djaoudi, K., Van Wambeke, F., Barani, A., Bhairy, N., Chevaillier, S., Desboeufs, K., Nunige, S., Labiadh, M., Henry des Tureaux, T., Lefèvre, D., Nouara, A., Panagiotopoulos, C., Tedetti, M., Pulido-Villena, E., 2020. Potential bioavailability of organic matter from atmospheric particles to marine heterotrophic bacteria. Biogeosciences, 17(24), 6271–6285. https://doi.org/10.5194/bg-17-6271-2020.

Elmquist M., Gustafsson, O., Andersson, P., 2004. Quantification of sedimentary black carbon using the chemothermal oxidation method: an evaluation of ex situ pretreatments and standard additions approach. Limnol. Oceanogr., 2, 417-427. https://doi.org/10.4319/lom.2004.2.417.

Fang, Y., Chen, Y., Huang, G., Hu, L., Tian, C., Xie, J., Lin, J., Lin, T., 2021. Particulate and Dissolved Black Carbon in Coastal China Seas: Spatiotemporal Variations, Dynamics, and Potential Implications. Environ. Sci. Technol., 55, 1, 788-796. https://doi.org/10.1021/acs.est.0c06386.

Fang, Y., B. Singh, B.P. Singh, E. Krull. 2014. Biochar carbon stability in four contrasting soils. Eur. J. Soil Sci., 65(1), 60-71. https://doi.org/10.1111/ejss.12094.

Fang, Z., Yang, W., Chen, M., Ma, H., 2017. Source and fate of dissolved black carbon in the western South China Sea during the Southwest monsoon prevailing season. J. Geophys. Res. Biogeosciences, 122. https://doi.org/10.1002/2017JG004014.

Farahani, V.J., Pirhadi, M., Sioutas, C., 2021. Are standardized diesel exhaust particles (DEP) representative of ambient particles in air pollution toxicological studies? Sci. Total Environ., 788, 147854. https://doi.org/10.1016/j.scitotenv.2021.147854.

Ferretto, N., Tedetti, M., Guigue, C., Mounier, S., Raimbault, P., Goutx, M., 2017. Spatio-temporal variability of fluorescent dissolved organic matter in the Rhône River delta and the Fos-Marseille marine area (France, NW Mediterranean Sea). Environ. Sci. Pollut. Res., 24, 4973-4989. https://doi.org/10.1007/s11356-016-8255-z.

Field, M., P., Cullen, J., T., Sherrell, R., M., 1999. Direct determination of 10 trace metals in 50 µL samples of coastal seawater using desolvating micronebulization sector field ICP-MS. J. Anal. At. Spectrom., 14, 1425-1431. https://doi.org/10.1039/A901693G.

Fourati, R., Tedetti, M., Guigue, C., Goutx, M., Garcia, N., Zaghden, H., Sayadi, S., Elleuch, B., 2018. Sources and spatial distribution of dissolved aliphatic and polycyclic aromatic hydrocarbons in surface coastal waters from the Gulf of Gabès (Tunisia, Southern Mediterranean Sea). Progr. Oceanogr., 163, 232-247. https://doi.org/10.1016/j.pocean.2017.02.001.

Fourrier, P., Dulaquais, G., Guigue, C., Giamarchi, P., Sarthou, G., Whitby, H., Riso, R., 2022. Characterization of the vertical size distribution, composition and chemical properties of dissolved organic matter in the (ultra)oligotrophic Pacific Ocean through a multi-detection approach. Mar. Chem., 240, 104068. https://doi.org/10.1016/j.marchem.2021.104068.

Ghosh, Prasenjit, Suparna Mukherji. 2021. Growth Kinetics of Pseudomonas Aeruginosa RS1 on Fluorene and Dibenzothiophene, Concomitant Degradation Kinetics and Uptake Mechanism. 3 Biotech 11(4), 195. https://doi.org/10.1007/s13205-021-02742-7.

Goranov, A.I., Wozniak, A.S., Bostick, K.W., Zimmerman, A.R., Mitra, S., Hatcher, P.G., 2022. Microbial labilization and diversification of pyrogenic dissolved organic matter. Biogeosciences, 19, 1491-1514. https://doi.org/10.5194/bg-19-1491-2022.

Guigue, C., Bigot, L., Turquet, J., Tedetti, M., Ferretto, N., Goutx, M., Cuet, P., 2015. Hydrocarbons in a coral reef ecosystem subjected to anthropogenic pressures (La Réunion Island, Indian Ocean). Environ. Chem., 12, 350-365. https://doi.org/10.1071/EN14194.

Helms, J.R., Stubbins, A., Ritchie, J.D., Minor, E.C., Kieber, D.J., Mopper, K., 2008. Absorption spectral slopes and slope ratios as indicators of molecular weight, source and photobleaching of chromophoric dissolved organic matter. Limnol. Oceanogr., 53, 955-969. https://doi.org/10.4319/lo.2008.53.3.0955.

Holmes, R.B., Aminot, A., Kérouel, R., Hooker, B.A., Peterson, B.J., 1999. A simple and precise method for measuring ammonium in marine and freshwater ecosystems. Canadian J. Fish. Aquat. Sci., 56, 1801-1808. https://doi.org/10.1139/f99-128.

Huguet, A., Vacher, L., Relexans, S., Saubusse, S., Froidefond, J.M., Parlanti, E., 2009. Properties of fluorescent dissolved organic matter in the Gironde Estuary. Org. Geochem., 40, 706-719. https://doi.org/10.1016/j.orggeochem.2009.03.002.

Huyen, T.T., Oanh, N.T.K., Nguyen Huy, L., Winijkul, E., Ha Chi, N., 2022. Impact of lowering fuel sulfur content on atmospheric emissions from shipping activities in a World Heritage Bay in Vietnam. Environ. Technol. Innov., 27, 102507. https://doi.org/10.1016/j.eti.2022.102507.

Im, J., Lee, C.M., Coates, J.T., 2008. Comparison of two reference black carbons using a planar PCB as a model sorbate. Chemosphere. 71, 621-628. https://doi.org/10.1016/j.chemosphere.2007.11.018.

Jaffé, R., Ding, Y., Niggemann, J., Vähätalo, A.V., Stubbins, A., Spencer, R.G.M., Campbell, J., Dittmar, T., 2013. Global charcoal mobilization from soils via dissolution and riverine transport to the oceans. Science, 340, 345-347. https://doi.org/10.1126/science.1231476.

Jones, M.W., Coppola, A.I., Santín, C., Dittmar, T., Jaffé, R., Doerr, S.H., Quine, T.A., 2020. Fires prime terrestrial organic carbon for riverine export to the global oceans. Nat. Comm., 11, 2791. https://doi.org/10.1038/s41467-020-16576-z.

Khodadad, C.L.M., Zimmerman, A.R., Green, S.J., Uthandi, S., Foster, J.S., 2011. Taxa-specific changes in soil microbial community composition induced by pyrogenic carbon amendments. Soil Biol. Biochem., 43(2), 385-92. https://doi.org/10.1016/j.soilbio.2010.11.005.

Kim, D., Young, T.M., Anastasio, C., 2013. Phototransformation rate constants of PAHs associated with soot particles. Sci. Tot. Environ., 443, 896-903. https://doi.org/10.1016/j.scitotenv.2012.11.055.

Kitidis, V., Stubbins, A.P., Uher, G., Goddard, R.C.U., Law, C.S., Woodward, E.M.S., 2006. Variability of chromophoric organic matter in surface waters of the Atlantic Ocean. Deep-Sea Res. II, 53, 1666-1684. https://doi.org/10.1016/j.dsr2.2006.05.009.

Kuzyakov, Y., Bogomolova, I., Glaser, B., 2014. Biochar Stability in Soil: Decomposition during Eight Years and Transformation as Assessed by Compound-Specific 14C Analysis. Soil Biol. Biochem., 70, 229-36. https://doi.org/10.1016/j.soilbio.2013.12.021.

Li, Rui, Junlin Li, Lulu Cui, Yu Wu, Hongbo Fu, Jianmin Chen, Mindong Chen. 2017. Atmospheric Emissions of Cu and Zn from Coal Combustion in China: Spatio-Temporal Distribution, Human Health Effects, and Short-Term Prediction. Environ. Poll., 229, 724-34. https://doi.org/10.1016/j.envpol.2017.05.068.

Li, L., Shen, X., Zhao, C., Liu, Q., Liu, X., Wu, Y.. 2019. Biodegradation of dibenzothiophene by efficient Pseudomonas Sp. LKY-5 with the production of a biosurfactant. Ecotox. Environ. Safety, 176, 50-57. https://doi.org/10.1016/j.ecoenv.2019.03.070.

Liu, Y., Lu, J., Chen, Y., Liu, Y., Ye, Z., Ge, X., 2020. Aqueous-Phase Production of Secondary Organic Aerosols from Oxidation of Dibenzothiophene (DBT). Atmosphere, 1, 151. https://doi.org/10.3390/atmos11020151.

Lønborg, C., Álvarez-Salgado, X.A.. 2012. Recycling versus export of bioavailable dissolved organic matter in the coastal ocean and efficiency of the continental shelf pump. Glob. Biogeochem. Cycl., 26(3), 2012GB004353. https://doi.org/10.1029/2012GB004353.

Mannino, A., Harvey, H.R., 2004. Black carbon in estuarine coastal ocean dissolved organic matter. Limnol. Oceanogr., 49, 735-740. https://doi.org/10.4319/lo.2004.49.3.0735.

Mari, X., Lefèvre, J., Torréton, J.P., Bettarel, Y., Pringault, O., Rochelle-Newall, E., Marchesiello, P., Menkes, C., Rodier, M., Migon, C., Motegi, C., Weinbauer, M.G., Legendre, L., 2014. Effects of soot deposition on particle dynamics and microbial processes in marine surface waters. Glob. Biogeochem. Cycles., 28(7), 662-678. https://doi.org/10.1002/2014GB004878.

Mari, X., Chu Van, T., Guinot, B., Brune, J., Lefebvre, J.-P., Raimbault, P., Dittmar, T., Niggemann, J., 2017. Seasonal dynamics of atmospheric and river inputs of black carbon, and impacts on biogeochemical cycles in Halong Bay, Vietnam. Elementa: Science of the Anthropocene, 5, 75. https://doi.org/10.1525/elementa.255.

Martias, C., Tedetti, M., Lantoine, F., Jamet, L., Dupouy, C., 2018. Characterization and sources of colored dissolved organic matter in a coral reef ecosystem subject to ultramafic erosion pressure (New Caledonia, Southwest Pacific). Sci. Tot. Environ., 616-617, 438-452. https://doi.org/10.1016/j.scitotenv.2017.10.261.

Masiello, C.A., 2004. New directions in black carbon organic geochemistry. Mar. Chem., 92, 201-213. https://doi.org/10.1016/j.marchem.2004.06.043.

Matuzawa, S., Nasser-Ali, L., Garrigues, P., 2001. Photolytic behavior of polycyclic aromatic hydrocarbons in diesel particulate matter deposited on the ground. Environ. Sci. Technol., 35, 3139-3143. https://doi.org/10.1021/es001606q.

Moran, M.A., Kujawinski, E.B., Stubbins, A., Fatland, R., Aluwihare, L.I., Buchan, A., Crump, B.C., Dorrestein, P.C., Dyhrman, S.T., Hess, N.J., Howe, B., Longnecker, K., Medeiros, P.M., Niggemann, J., Obernosterer, I., Repeta, D.J., Waldbauer, J.R., 2016. Deciphering ocean carbon in a changing world. Proc. Natl. Acad. Sci. U.S.A, 113, 3143-3151. https://doi.org/10.1073/pnas.1514645113.

Mori, Y., Nishioka, J., Fujio, S., Yamashita, Y., 2021. Transport of dissolved black carbon from marginal sea sediments to the western North Pacific. Progr. Oceanogr., 193, 102552. https://doi.org/10.1016/j.pocean.2021.102552.

Murphy, K.R., Stedmon, C.A., Waite, T.D., Ruiz, G.M., 2008. Distinguishing between terrestrial and autochthonous organic matter sources in marine environments using fluorescence spectroscopy. Mar. Chem., 108, 40-58. https://doi.org/10.1016/j.marchem.2007.10.003.

Nakane, M., Ajioka, T., Yamashita, Y., 2017. Distribution and sources of dissolved black carbon in surface waters of the Chukchi Sea, Bering Sea, and the North Pacific Ocean. Front. Earth Sci., 5, 34. https://doi.org/10.3389/feart.2017.00034.

Neff, J.M., 2002. Bioaccumulation in marine organisms: effect of contaminants from oil well produced water. Elsevier, 241-318. ISBN: 0-08-043716-8.

Nyholm, N., Kristensen, P., 1991. Screening Methods for Assessment of Biodegradability of Chemicals in Seawater – Results from a Ring Test. Ecotoxicol. Environ. Saf., 23, 161-172.

Oeder S, Kanashova T, Sippula O, Sapcariu SC, Streibel T, Arteaga-Salas JM, et al. (2015) Particulate Matter from Both Heavy Fuel Oil and Diesel Fuel Shipping Emissions Show Strong Biological Effects on Human Lung Cells at Realistic and Comparable In Vitro Exposure Conditions. PLoS ONE 10(6), e0126536. https://doi.org/10.1371/journal.pone.0126536.

Ohno, T., 2002. Fluorescence inner-filtering correction for determining the humification index of dissolved organic matter. Environ. Sci. Technol., 36, 742-746. https://doi.org/10.1021/es0155276.

Popovicheva, O., Kireeva, E., Shonija, N., Zubareva, N., Persiantseva, N., Tishkova, V., et al. (2009). Ship particulate pollutants: Characterization in terms of environmental implication. J. Environ. Monitor., 11(11), 2077-2086. https://doi.org/10.1039/B908180A.

Qi, Y., Fu, W., Tian, J., Luo, C., Shan, S., Sun, S., Ren, P., Zhang, H., Liu, J., Zhang, X., Wang, X., 2020. Dissolved black carbon is not likely a significant refractory organic carbon pool in rivers and oceans. Nat. Commun., 11, 5051. https://doi.org/10.1038/s41467-020-18808-8.

Quéméneur, M., Chifflet, S., Akrout, F., Bellaaj-Zouari, A., Blhassen, M., 2022. Impact of cigarette butts on microbial diversity and dissolved trace metals in coastal marine sediment. Estuar. Coast. Shelf Sci., 240. https://doi.org/10.1016/j.ecss.2020.106785.

Raimbault, P., Pouvesle, W., Sempéré, R., 1999. Wet-oxidation and automated colorimetry for simultaneous determination of organic carbon, nitrogen and phosphorus dissolved in seawater. Mar. Chem., 66, 161-169. https://doi.org/10.1016/S0304-4203(99)00038-9.

Revsbech, N., P., 1989. An oxygen microsensor with a guard cathode. Limnol. Oceanogr., 34, 474-478.

Saiz-Lopez, A., Saunders, R.W., Joseph, D.M., Ashworth, S.H., Plane, J.M.C., 2004. Absolute absorption cross-section and photolysis rate of I2. Atmos. Chem. Phys., 4, 1443-1450. https://doi.org/10.1029/2003GL019215.

Seidel, M., Beck, M., Riedel, T., Waska, H., Suryaputra, I.G.N.A., Schnetger, B., Niggemann, J., Simon, M., 2014. Biogeochemistry of dissolved organic matter in an anoxic intertidal creek bank. Geochim. Cosmochim. Acta, 140, 418-434. https://doi.org/10.1016/j.gca.2014.05.038.

Singh, P., DeMarini, D.M., Dick, C.A., Tabor, D.G., Ryan, J.V., Linak, W.P., Kobayashi, T., Gilmour, M.I., 2004. Sample characterization of automobile and forklift diesel exhaust particles and comparative pulmonary toxicity in mice. Environ. Health Persp., 112, 820-825. https://doi.org/10.1289/ehp.6579.

Smith, D.C., Azam, F. (1992). A simple, economical method for measuring bacterial protein synthesis rates in seawater using 3H-leucine. Mar. Microb. Food Webs, 6(2), 107-114.

Sohrin, R., Sempéré, R., 2005. Seasonal variation in total organic carbon in the Northeast Atlantic in 2000-2001. J. Geophys. Res. Oceans, 110(C10). https://doi.org/10.1029/2004JC002731.

Stedmon, C.A., Bro, R., 2008. Characterizing dissolved organic matter fluorescence with parallel factor analysis: a tutorial. Limnol. Oceanogr. Methods, 6, 572-579. https://doi.org/10.4319/lom.2008.6.572.

Stubbins, A., Niggemann, J., Dittmar, T., 2012. Photolability of deep ocean dissolved black carbon. Biogeosciences, 9, 1661-1670. https://doi.org/10.5194/bg-9-1661-2012.

Stubbins, A., Spencer, R.G.M., Mann, P.J., Holmes, R.M., McClelland, J.W., Niggemann, J., Dittmar, T., 2015. Utilizing colored dissolved organic matter to derive dissolved black carbon export by arctic rivers. Front. Earth Sci., 3, 63. https://doi.org/10.3389/feart.2015.00063.

Taylor, B.W., Keep, C.F., Hall, R.O., Koch, B.J., Tronstad, L.M., Flecker, A.S., Ulseth, A.J., 2007. Improving the fluorometric ammonium method: matrix effects, background fluorescence, and standard additions. J. North Am. Benthol. Soc., 26(2), 167-177. https://doi.org/10.1899/0887-3593(2007)26[167:ITFAMM]2.0.CO;2.

Tedetti, M., Bigot, L., Turquet, J., Guigue, C., Ferretto, N., Goutx, M., Cuet, P., 2020. Influence of freshwater discharges on biogeochemistry and benthic communities in a coral reef ecosystem (La Réunion Island, Indian Ocean). Front. Mar. Sci., 7, 596165. https://doi.org/10.3389/fmars.2020.596165.

Tedetti, M., Longhitano, R., Garcia, N., Guigue, C., Ferretto, N., Goutx, M., 2012. Fluorescence properties of dissolved organic matter in coastal Mediterranean waters influenced by a municipal sewage effluent (Bay of Marseilles, France). Environ. Chem., 9, 438-449. https://doi.org/10.1071/EN12081.

Tedetti, M., Marie, L., Röttgers, R., Rodier, M., Van Wambeke, F., Helias, S., Caffin, M., Cornet-Barthaux, V., Dupouy, C., 2016. Evolution of dissolved and particulate chromophoric materials during the VAHINE mesocosm experiment in the New

Caledonian coral lagoon (south-west Pacific). Biogeosciences, 13, 3283-3303. https://doi.org/10.5194/bg-13-3283-2016.

Van Wambeke, F., Pulido, E., Dinasquet, J., Djaoudi, K., Engel, A., Garel, M., Guasco, S., Nunige, S., Taillandier, V., Zäncker, B., & Tamburini, C., (2020). Spatial patterns of biphasic ectoenzymatic kinetics related to biogeochemical properties in the Mediterranean Sea. Biogeosciences. https://doi.org/10.5194/bg-2020-253.

Velis, C.A., Cook, E., 2021. Mismanagement of plastic waste through open burning with emphasis on the global south: a systematic review of risks to occupational and public health. Environ. Sci. Technol., 55, 7186-7207. https://doi.org/10.1021/acs.est.0c08536.

Wagner, S., Brandes, J., Spencer, R.G.M., Ma, K., Rosengard, S.Z., Mauro, J., Moura, S., Stubbins, A., 2019. Isotopic composition of oceanic dissolved black carbon reveals non-riverine source. Nat. Commun., 10, 5064. https://doi.org/10.1038/s41467-019-13111-7.

Wagner, S., Coppola, A.I., Stubbins, A., Dittmar, T., Niggemann, J., Drake, T.W., Seidel, M., Spencer, R.G.M., Bao, H., 2021. Questions remain about the biolability of dissolved black carbon along the combustion continuum. Nat. Commun., 12, 4281. https://doi.org/10.1038/s41467-021-24477-y.

Wagner, S., Jaffé, R., Stubbins A., 2018. Dissolved black carbon in aquatic ecosystems. Limnol. Oceanogr. Letters, 3, 168-185. https://doi.org/10.1002/lol2.10076.

Wagner, S., Ding, Y., Jaffé, R., 2017. A new perspective on the apparent solubility of dissolved black carbon. Front. Earth Sci., 5, 75. https://doi.org/10.3389/feart.2017.00075.

Weishaar, J.L., Aiken, G.R., Bergamaschi, B.A., Fram, M.S., Fujii, R., Mopper, K., 2003. Evaluation of specific ultraviolet absorbance as an indicator of the chemical composition and reactivity of dissolved organic carbon. Environ. Sci. Technol., 37, 4702-4708. https://doi.org/10.1021/es030360x.

Wennberg, A. C., Meland, S., Grung, M., Lillicrap, A., 2022. Unravelling reasons for variability in the OECD 306 marine biodegradation test. Chemosphere, 300, 134476. https://doi.org/10.1016/j.chemosphere.2022.134476.

Wright, M.E., Klein, A.D., Stesniak, E.J., 1991. A diesel exhaust filter system for industrial diesel forklifts (No. 911852). SAE Technical Paper.

Yamashita, Y., Kojima, D., Yoshida, N., Shibata, H., 2021. Relationships between dissolved black carbon and dissolved organic matter in streams. Chemosphere, 271, 129824. https://doi.org/10.1016/j.chemosphere.2021.129824.

Yamashita, Y., Nakane, M., Mori, Y., Nishioka, J., Ogawa, H., 2022. Fate of dissolved black carbon in the deep Pacific Ocean. Nat. Commun., 13, 307. https://doi.org/10.1038/s41467-022-27954-0.

Zhao, B., Liang, X., Wang, K., Li, T., $LD_{SHIP}$, X., Zhang, S., 2022. Impact of sulfur functional groups on physicochemical properties and oxidation reactivity of diesel soot particles. Fuel, 327, 125041, https://doi.org/10.1016/j.fuel.2022.125041.

Zhong, G., Sun, Y., Xiaofei, G., Yi, X., Zhang, G., 2019. Benzene polycarboxylic acid characterisation of polyaromatics in ambient aerosol: Method development. Atmos. Environ., 211, https://doi.org/10.1016/j.atmosenv.2019.04.057.

Zimmermann, M., Bird, M.I., Wurster, C., Saiz, G., Goodrick, I., Barta, J., Capek, P., Santruckova, H., Smernik, R., 2012. Rapid degradation of pyrogenic carbon. Global Change Biology 18(11), 3306-16. https://doi.org/10.1111/j.1365-2486.2012.02796.x.

Ziolkowski, L.A., Druffel, E.R.M., 2010. Aged black carbon identified in marine dissolved organic carbon. Geophys. Res. Lett., 37, L16601. https://doi.org/10.1029/2010GL043963.

Ziolkowski, L., Chamberlin, A., Greaves, J., Druffel, E., 2011. Quantification of black carbon in marine systems using the benzene polycarboxylic acid method: A mechanistic and

yield study. Limnol. Oceanogr. Methods, 9, 140-149. https://doi.org/10.4319/lom.2011.9.140.

Zsolnay, A., Baigar, E., Jimenez, M., Steinweg, B., Saccomandi, F., 1999. Differentiating with fluorescence spectroscopy the sources of dissolved organic matter in soils subjected to drying. Chemosphere, 38, 45-50. https://doi.org/10.1016/S0045-6535(98)00166-0.

**Table 1.** Volumes (in mL) of the different solutions added (natural DOM, BC-derived DOM stock solutions, bacterial inoculum, $NO_3^-$ and $PO_4^{3-}$ stock solutions) for preparation of the incubation solutions used to carry out the 90-day experiment on biodegradation of BC-derived DOM by marine heterotrophic prokaryotes under five treatments in triplicate (three bottles): C (control), $D_{REF}$ (diesel), $D_{REF\text{-}OX}$ (oxidized diesel), $D_{SHIP}$ (ship soot), and $D_{SHIP\text{-}Ab}$ ("abiotic" ship soot).

| | **C** | **$D_{REF}$** | **$D_{REF\text{-}OX}$** | **$D_{SHIP}$** | **$D_{SHIP\text{-}Ab}$** |
|---|---|---|---|---|---|
| Natural DOM | 3270 | 2900 | 2980 | 3100 | 1900 |
| BC-derived DOM stock solutions | 0 | 370 | 290 | 170 | 100 |
| Bacterial inoculum | 60 | 60 | 60 | 60 | 0 |
| $NO_3^-$ stock solution (39 mM) | 1 | 0.5 | 0.6 | 0.8 | 0.5 |
| $PO_4^{3-}$ stock solution (5.7 mM) | 1 | 0 | 0.5 | 0.9 | 0.5 |
| Total vol. of incubation solutions | 3332 | 3331 | 3331 | 3332 | 2000 |

**Table 2.** Content and CDOM/FDOM characteristics of BC-derived DOM solutions at the start (T0) of the biodegradation experiment for the five treatments: C (control), $D_{REF}$ (diesel), $D_{REF\text{-}OX}$ (oxidized diesel), $D_{SHIP}$ (ship soot), and $D_{SHIP\text{-}Ab}$ ("abiotic" ship soot). Values are the average and standard deviation of the triplicates (three bottles) for each treatment. For each parameter, values with different superscript letters (a, b, c or d) are significantly different (t-test, $p < 0.05$).

| **Final concentrations** | **C** | **$D_{REF}$** | **$D_{REF\text{-}OX}$** | **$D_{SHIP}$** | **$D_{SHIP\text{-}Ab}$** |
|---|---|---|---|---|---|
| DOC (µM) | 74 ± 1$^{a}$ | 264 ± 3$^{b}$ | 244 ± 4$^{c}$ | 265 ± 3$^{b}$ | 266 ± 1$^{b}$ |
| DON (µM) | 2.9 ± 1.7$^{a}$ | 9.1 ± 0.2$^{b}$ | 8.4 ± 0.8$^{b}$ | 11.8 ± 0.2$^{c}$ | 11.7 ± 0.2$^{c}$ |
| DOP (µM) | 0.1 ± 0.1$^{a}$ | 0.2 ± 0.0$^{a}$ | 0.2 ± 0.0$^{a}$ | 0.1 ± 0.0$^{a}$ | 0.1 ± 0.0$^{a}$ |
| DBC (µg C $L^{-1}$) | 12 ± 2$^{a}$ | 939 ± 82$^{b}$ | 869 ± 121$^{b}$ | 974 ± 70$^{b}$ | 940 ± 172$^{b}$ |
| DBC/DOC (%) | 1.3 | 29.6 | 29.6 | 31.0 | 29.5 |
| d-PAHs (ng $L^{-1}$) | 13.7 ± 2.3$^{a}$ | 26.9 ± 9.5$^{b}$ | 23.1 ± 1.6$^{b}$ | 309 ± 92$^{c}$ | 258 ± 69$^{c}$ |
| d-TM (µg $L^{-1}$) | 29.7 ± 18.5$^{a}$ | 36.2 ± 1.0$^{a}$ | 31.6 ± 2.3$^{a}$ | 34.0 ± 2.0$^{a}$ | 30.6 ± 1.8$^{a}$ |
| $Si(OH)_4$ (µM) | 9.5 ± 0.5$^{a}$ | 15.2 ± 1.1$^{b}$ | 10.7 ± 1.6$^{a}$ | 9 ± 0.4$^{a}$ | 5.5 ± 0.2$^{c}$ |
| $NO_3^-$ (µM) | 12.6 ± 0.1$^{a}$ | 7.4 ± 0.0$^{b}$ | 8.5 ± 0.2$^{c}$ | 10 ± 0.1$^{d}$ | 10 ± 0.0$^{d}$ |
| $NO_2^-$ (µM) | 0.0 ± 0.0$^{a}$ | 2.0 ± 0.0$^{b}$ | 0.8 ± 0.0$^{c}$ | 0.3 ± 0.0$^{d}$ | 0.3 ± 0.0$^{d}$ |
| $NH_4^+$ (µM) | 0.1 ± 0.1$^{a}$ | 2.4 ± 0.1$^{b}$ | 2.9 ± 0.1$^{c}$ | 2.3 ± 0.1$^{b}$ | 2.3 ± 0.1$^{b}$ |
| $PO_4^{3-}$ (µM) | 1.8 ± 0.0$^{a}$ | 1.6 ± 0.0$^{b}$ | 1.6 ± 0.0$^{c}$ | 1.7 ± 0.0$^{d}$ | 1.8 ± 0.0$^{d}$ |
| **CDOM/FDOM indices** | **C** | **$D_{REF}$** | **$D_{REF\text{-}OX}$** | **$D_{SHIP}$** | **$D_{SHIP\text{-}Ab}$** |
| HIX | 2.0 ± 0.0$^{a}$ | 37.3 ± 8.6$^{b}$ | 34.5 ± 2.0$^{b}$ | 49.4 ± 1.9$^{c}$ | 49.8 ± 1.4$^{c}$ |
| BIX | 1.0 ± 0.1$^{a}$ | 0.9 ± 0.0$^{b}$ | 0.8 ± 0.0$^{c}$ | 0.5 ± 0.0$^{d}$ | 0.5 ± 0.0$^{d}$ |
| $SUVA_{254}$ (L mg $C^{-1}$ $m^{-1}$) | 1.7 ± 0.1$^{a}$ | 13.9 ± 0.4$^{b}$ | 11.5 ± 0.2$^{c}$ | 18.8 ± 0.1$^{d}$ | 18.7 ± 0.3$^{d}$ |
| $a_{CDOM}(254)$ ($m^{-1}$) | 1.6 ± 0.1$^{a}$ | 43.2 ± 0.5$^{b}$ | 33.7 ± 0.1$^{c}$ | 60.0 ± 0.3$^{d}$ | 59.7 ± 1.0$^{d}$ |

DOC: dissolved organic carbon; DON: dissolved organic nitrogen; DOP: dissolved organic phosphorus; DBC: dissolved black carbon; d-PAHs: dissolved polycyclic aromatic hydrocarbons; d-TM: dissolved metallic trace elements; $Si(OH)_4$: silicates; $NO_3^-$: nitrates; $NO_2^-$: nitrites; $NH_4^+$: ammonium; $PO_4^{3-}$: phosphates; HIX: humic index; BIX: biological index; $SUVA_{254}$: specific UV absorbance at 254 nm; $a_{CDOM}(254)$: CDOM absorption coefficient at 254 nm.

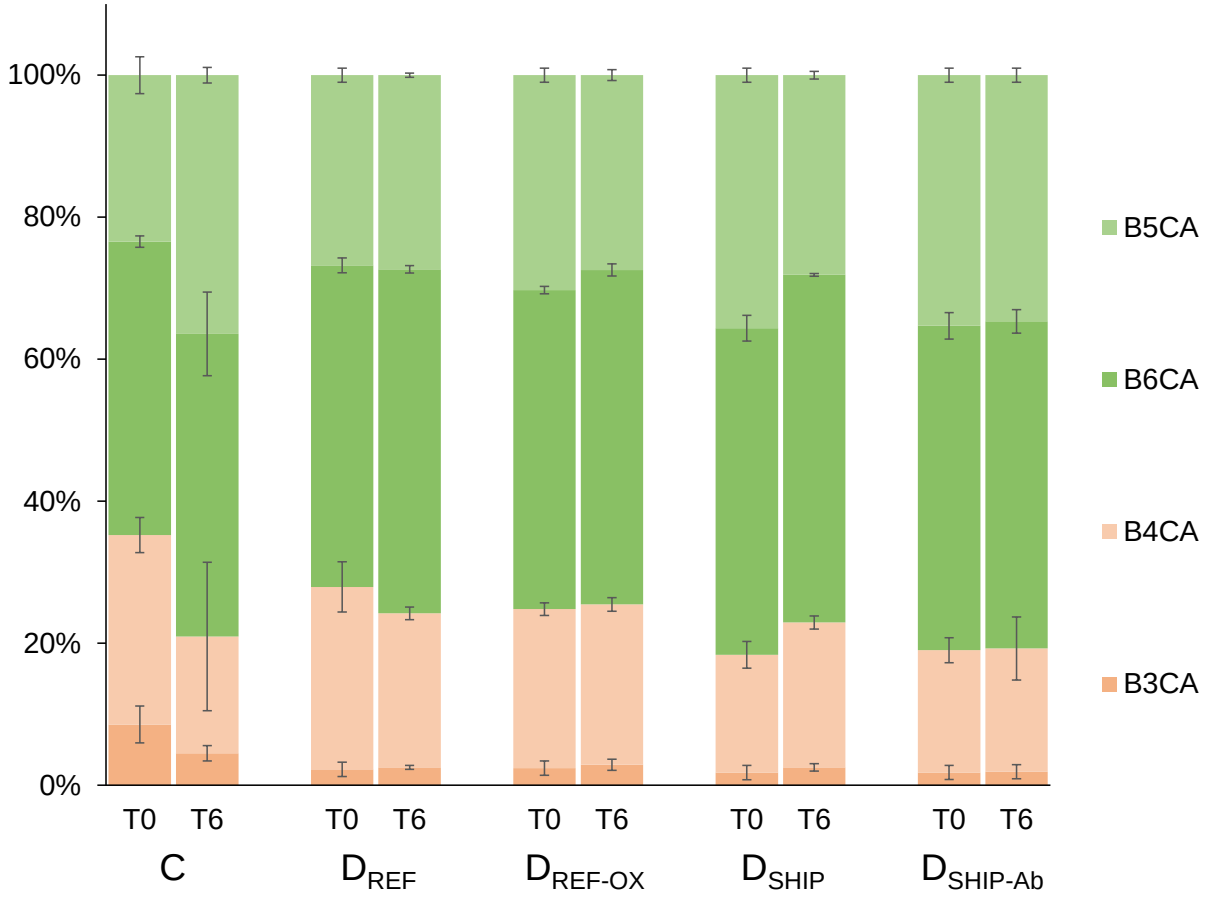


**Figure 1.** Relative abundances (in %) of benzenepolycarboxylic acids (BPCAs, in µg C $L^{-1}$) at (a) the start (T0) and (b) the end (T6: 90 days) of the BC-derived DOM biodegradation experiment for the four biotic treatments: C (control), $D_{REF}$ (diesel), $D_{REF\text{-}OX}$ (oxidized diesel), $D_{SHIP}$ (ship soot), and $D_{SHIP\text{-}Ab}$ ("abiotic" ship soot). The green color gradient charts molecules with a low number of carboxyl groups (B3CA, B4CA) and the orange color gradient charts molecules with a high number of carboxyl groups (B5CA, B6CA).

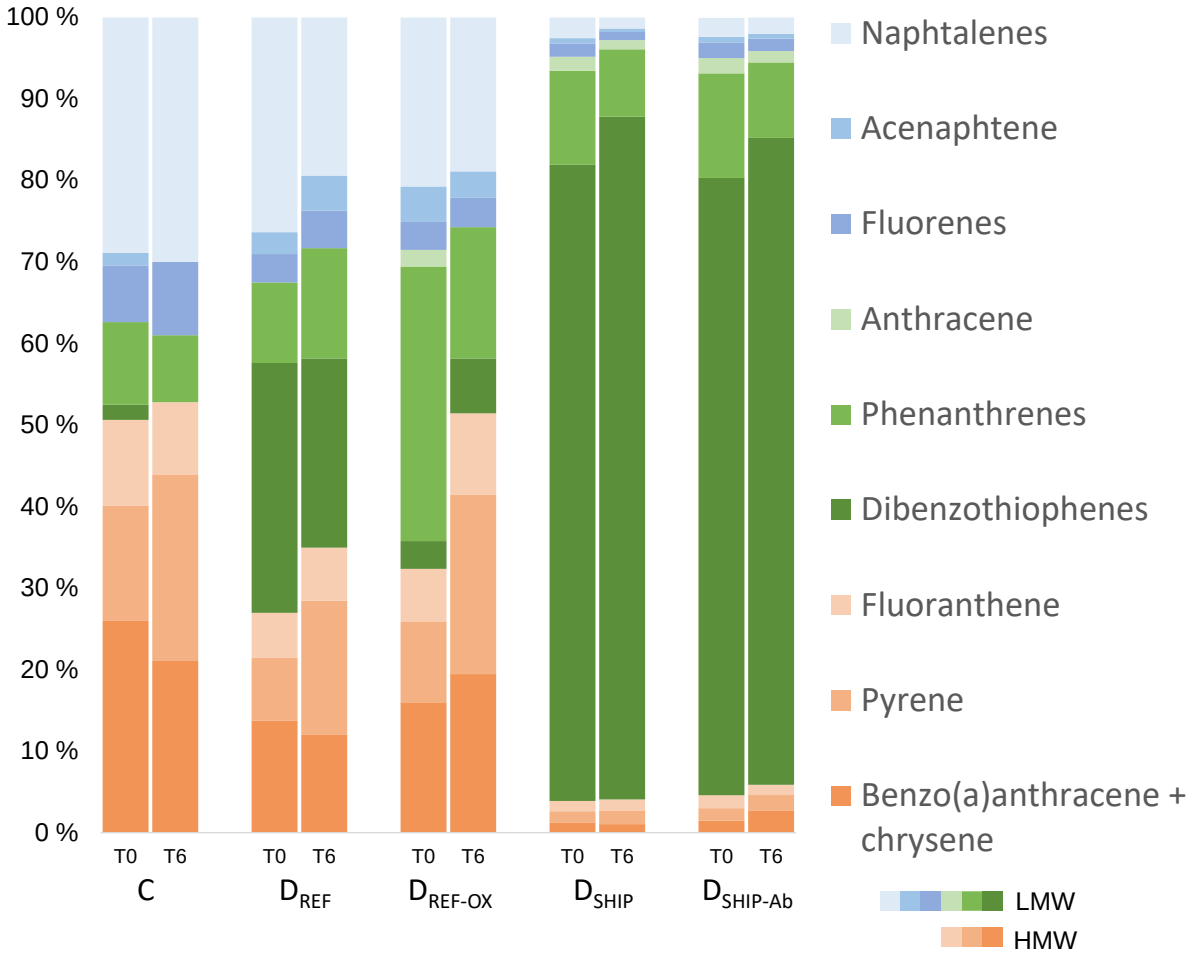


**Figure 2.** Relative abundances (in %) of dissolved polycyclic aromatic hydrocarbons (d-PAHs, in ng $L^{-1}$) at (a) the start (T0) and (b) the end (T6: 90 days) of the BC-derived DOM biodegradation experiment for the four biotic treatments: C (control), $D_{REF}$ (diesel), $D_{REF-OX}$ (oxidized diesel), $D_{SHIP}$ (ship soot), and $D_{SHIP-Ab}$ ("abiotic" ship soot). The green color gradient charts low-molecular-weight (LMW) PAHs, and the orange color gradient charts high-molecular-weight (HMW) PAHs.

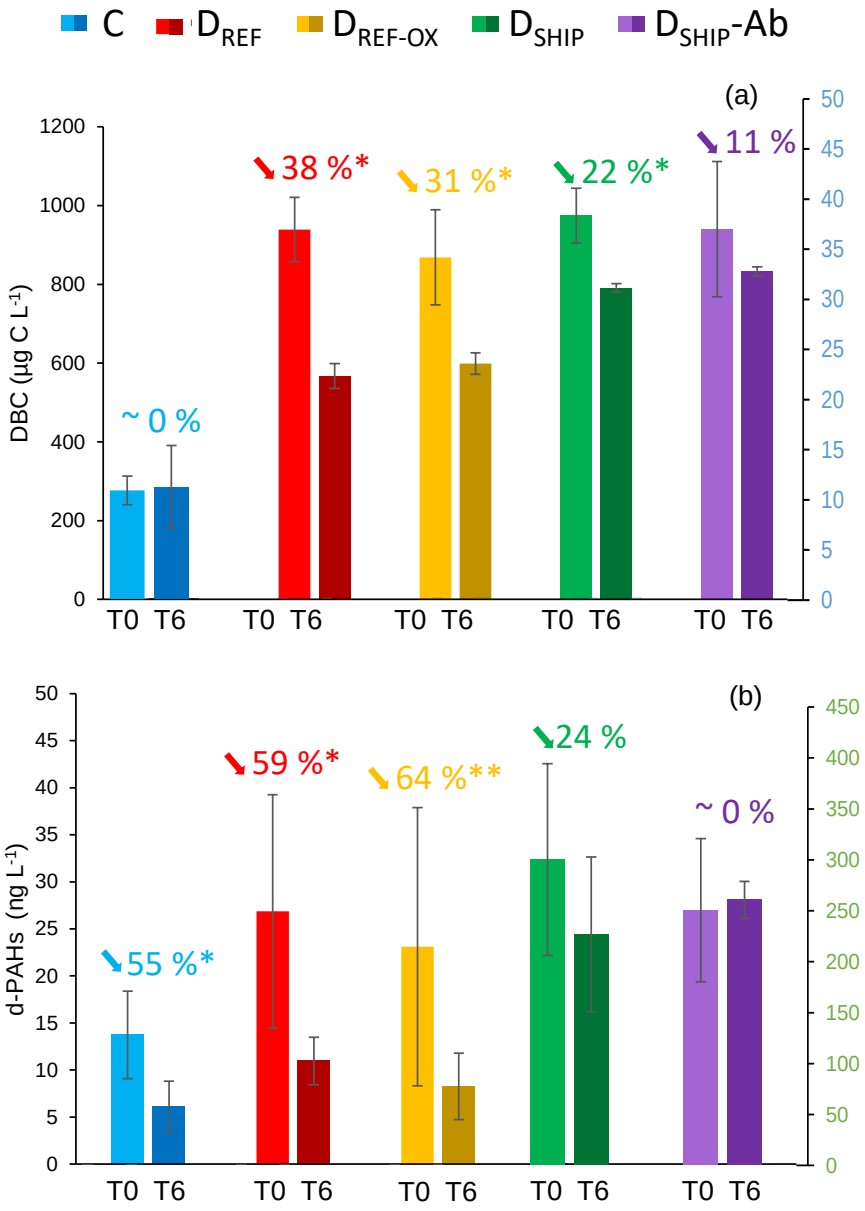


| | | C | $D_{REF}$ | $D_{REF-OX}$ | $D_{SHIP}$ | $D_{SHIP-Ab}$ |
|---|---|---|---|---|---|---|
| DOC (µM) | Start | 75.0 ± 0 | 263.0 ± 2.8 | 242.0 ± 1.4 | 265.0 ± 4.2 | 265.5 ± 0.7 |
| | End | 73.0 ± 0 | 215.5 ± 4.9 | 197.0 ± 2.8 | 244.0 ± 2.8 | 261 ± 5.7 |

**Figure 3.** Concentrations of (a) dissolved black carbon (DBC, in µg C $L^{-1}$) and (b) dissolved PAHs (d-PAHs, in ng $L^{-1}$) at the start (T0) and the end (T6: 90 days) of the BC-derived DOM biodegradation experiment for the four biotic treatments: C (control), $D_{REF}$ (diesel), $D_{REF-OX}$ (oxidized diesel), $D_{SHIP}$ (ship soot), and $D_{SHIP-Ab}$ ("abiotic" ship soot). The percent decrease between T0 and T6 is shown. When associated with an *, the figure reflects a significant

decrease between T0 and T6 (t-test, $p < 0.05$ for * and $p < 0.1$ for **). Second vertical scales: (a) in blue for the C treatment, (b) in green for the $D_{SHIP}$ treatment. Error bars correspond to the standard deviation of the triplicates.

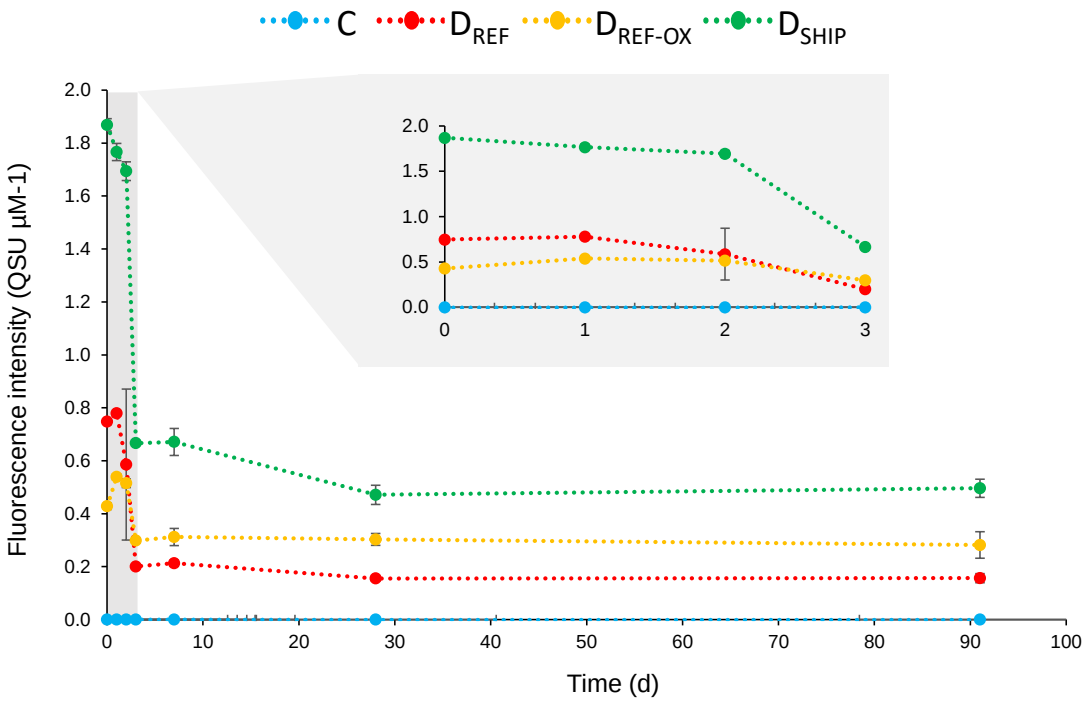

**Figure 4.** Time-course of the fluorescence intensities of the C2 FDOM component ($\lambda_{Ex}/\lambda_{Em}$: 305/432 nm) normalized to DOC (in QSU $\mu M^{-1}$) throughout the BC-derived DOM biodegradation experiment (up to T6: 90 days), with a focus on the first 3 days (up to T3: 3 days), for the four biotic treatments: C (control), $D_{REF}$ (diesel), $D_{REF\text{-}OX}$ (oxidized diesel), and $D_{SHIP}$ (ship soot). Error bars correspond to the standard deviation of the triplicates.

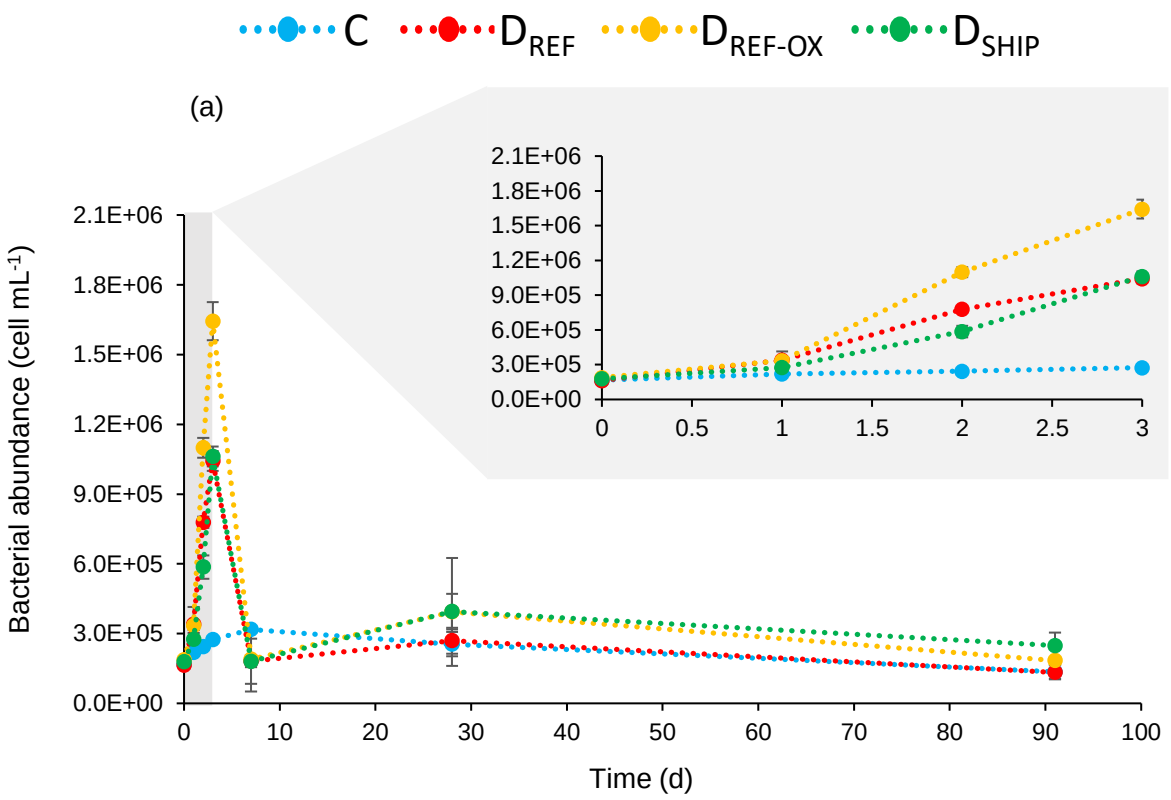

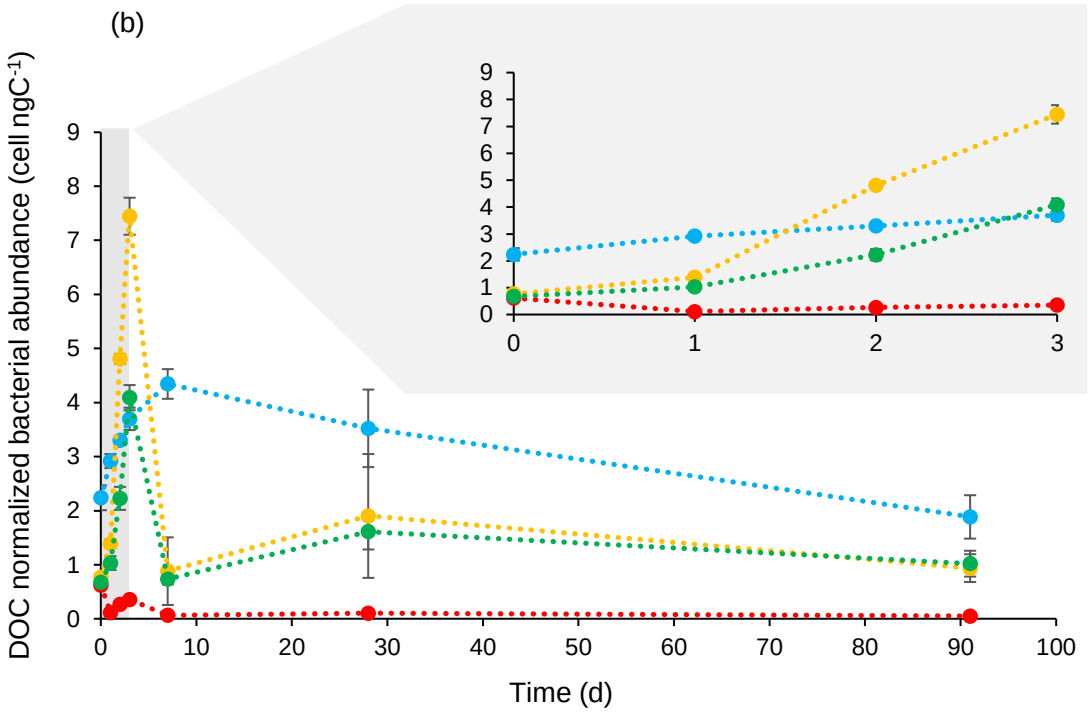


**Figure 5.** Time-course of (a) bacterial abundance (cell $mL^{-1}$) and (b) bacterial abundance normalized to DOC (cell ng $C^{-1}$) throughout the BC-derived DOM biodegradation experiment (up to T6: 90 days), with a focus on the first 3 days (up to T3: 3 days), for the four biotic treatments: C (control), $D_{REF}$ (diesel), $D_{REF\text{-}OX}$ (oxidized diesel), and $D_{SHIP}$ (ship soot). Error bars correspond to the standard deviation of the triplicates.

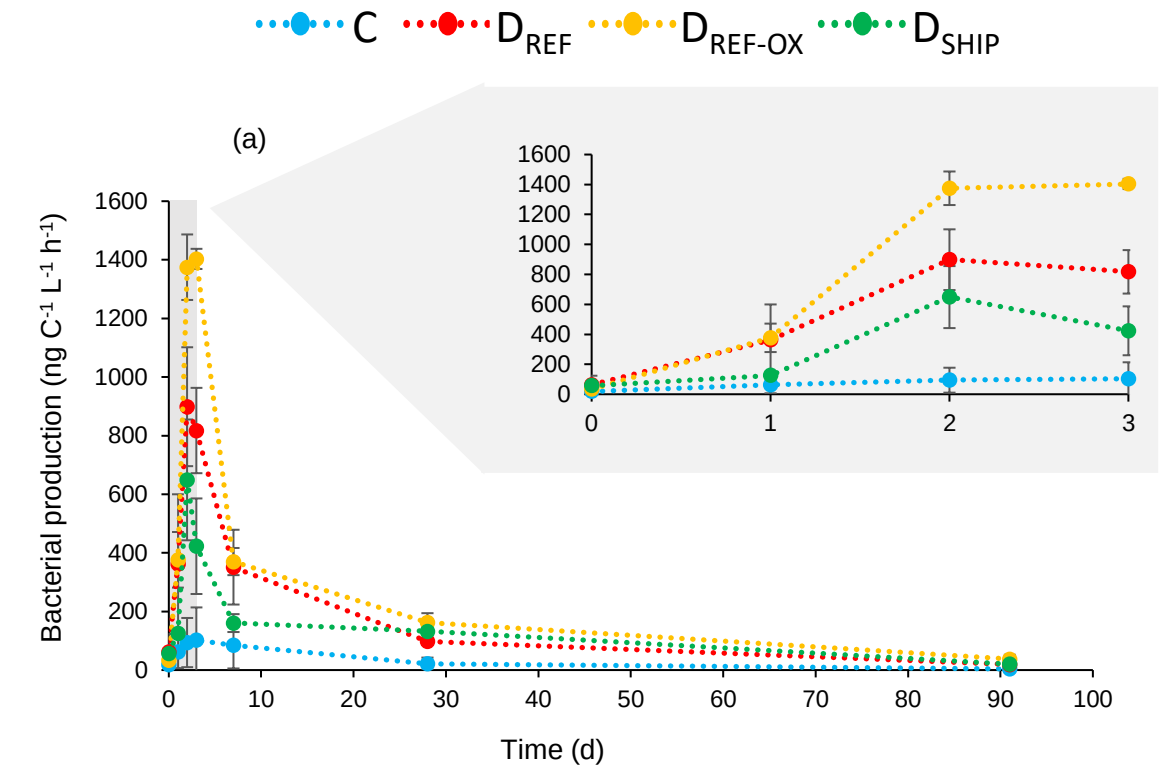
C
D_REF
D_REF-OX
D_SHIP
(a)
Bacterial production (ng C-1 L-1 h-1)
Time (d)

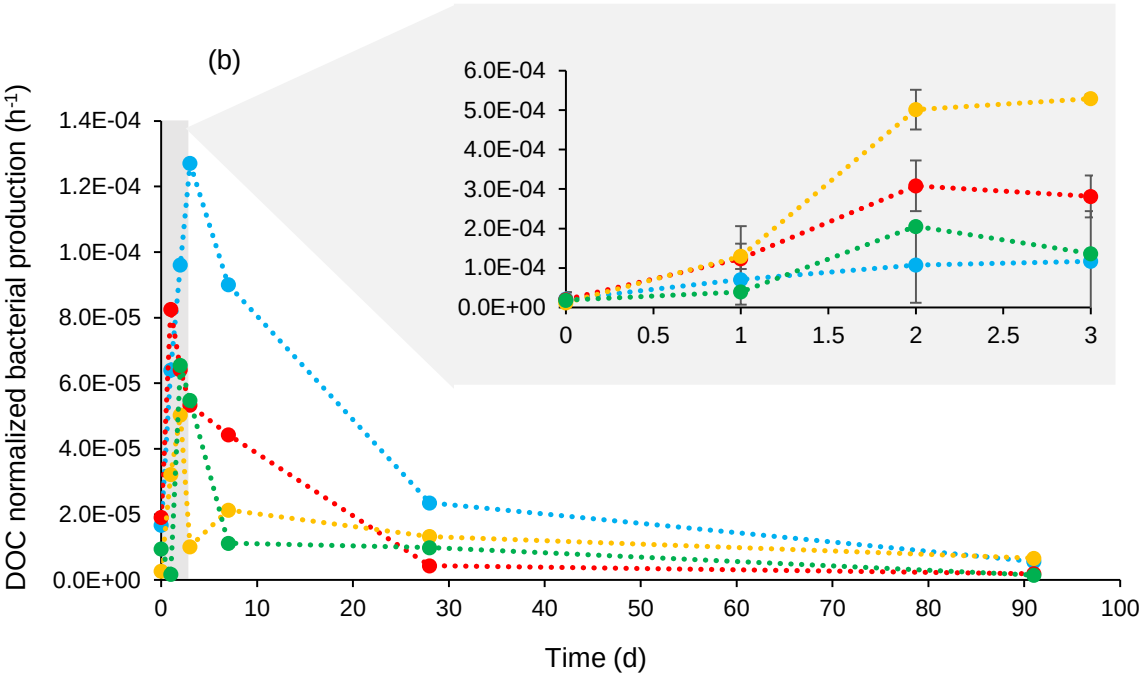
(b)
DOC normalized bacterial production (h-1)
Time (d)

**Figure 6.** Time-course of (a) bacterial production (ng C $L^{-1}$ $h^{-1}$) and (b) bacterial production normalized to DOC ($h^{-1}$) (b) throughout the BC-derived DOM biodegradation experiment (up to T6: 90 days), with a focus on the first 3 days (up to T3: 3 days), for the four biotic treatments: C (control), $D_{REF}$ (diesel), $D_{REF\text{-}OX}$ (oxidized diesel), and $D_{SHIP}$ (ship soot). Error bars correspond to the standard deviation of the triplicates.

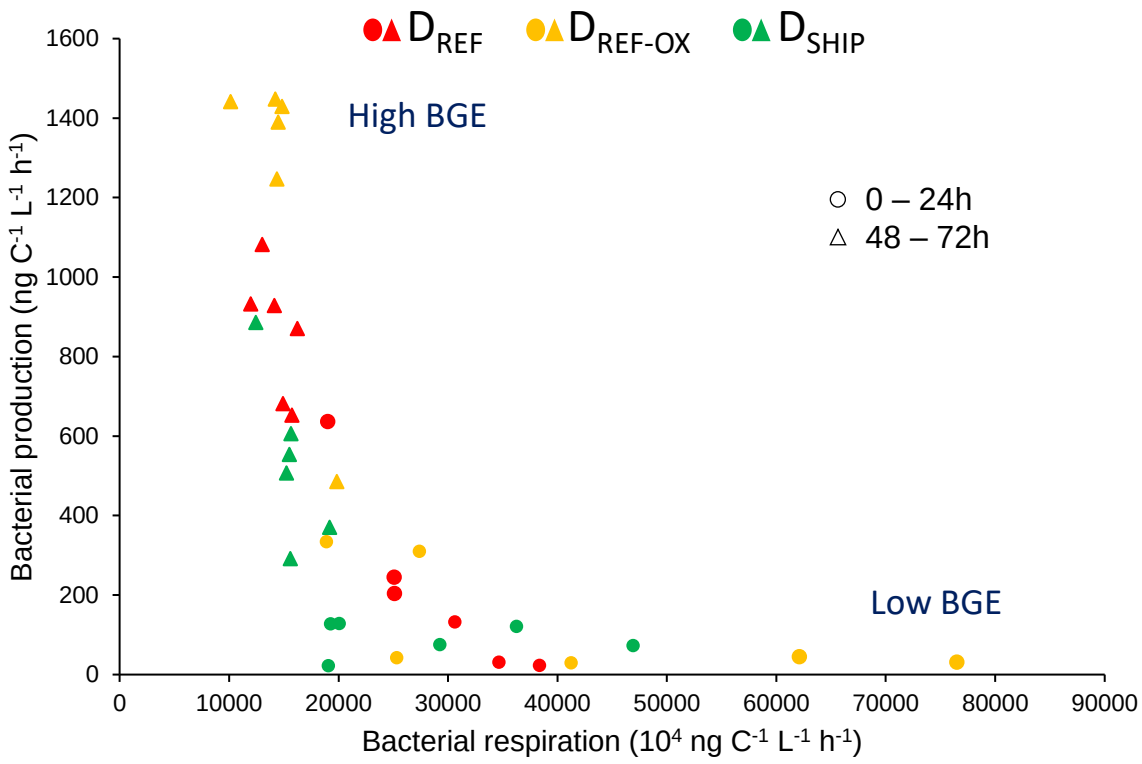


**Figure 7.** Relationship (power function) between bacterial respiration (ng $C^{-1}$ $L^{-1}$ $h^{-1}$) and bacterial production (ng $C^{-1}$ $L^{-1}$ $h^{-1}$) for the $D_{REF}$, $D_{REF-OX}$ and $D_{SHIP}$ treatments from T0 to T3 of the BC-derived DOM biodegradation experiment (n = 36).

# Assessing the bioavailability of black carbon-derived dissolved organic matter for marine heterotrophic prokaryotes

Pauline L. Martinot[a, c]*, Catherine Guigue[a, c], Sandrine Chifflet[a], Philippe Cuny[a], Aude Barani[a], Morgane Didry[a], Clara Dignan[b], Léa Guyomarc'h[a], Nathalie Pradel[a], Olivier Pringault[a], France Van Wambeke[a], Cam Tu Vu[c], Xavier Mari[a, c], Marc Tedetti[a, c]

[a] Aix Marseille Univ., Université de Toulon, CNRS, IRD, MIO, Marseille, France

[b] Université de Toulon, Aix Marseille Univ., CNRS, IRD, MIO, Toulon, France

[c] Water - Environment - Oceanography (WEO) Department, University of Science and Technology of Hanoi (USTH), Vietnam Academy of Science and Technology (VAST), Hanoi, Vietnam

* Corresponding author; pauline.martinot@mio.osupytheas.fr

## Supplementary Material

The supplementary material contains 19 pages, and includes 7 tables, 11 figures and 3 texts.

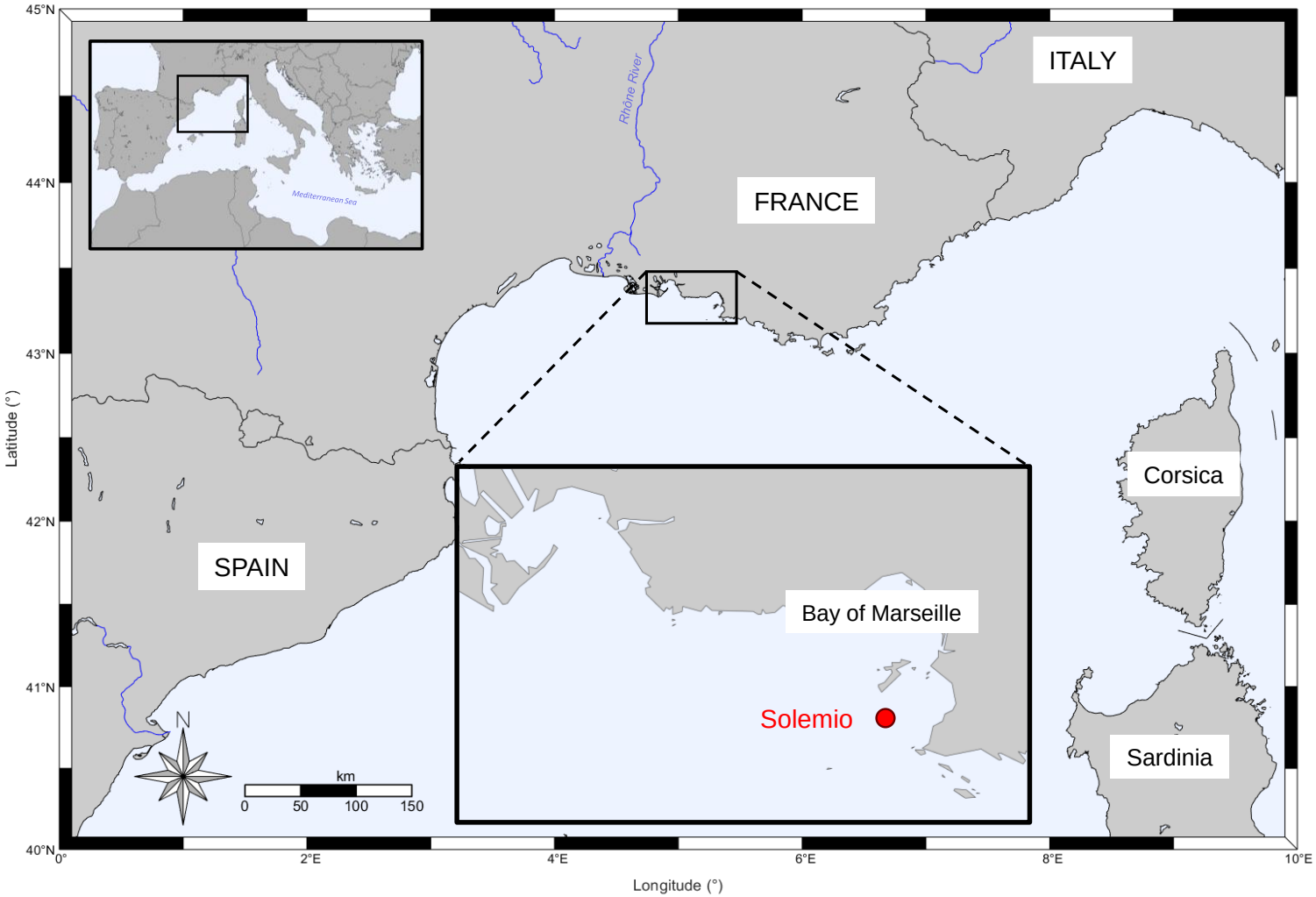


**Figure S1.** Location of the SOLEMIO station in the bay of Marseille (south of France) in the Northwestern Mediterranean Sea. SOLEMIO is part of the French national network of coastal observation SOMLIT (Service d'Observation en Milieu LITtoral; https://www.somlit.fr/).

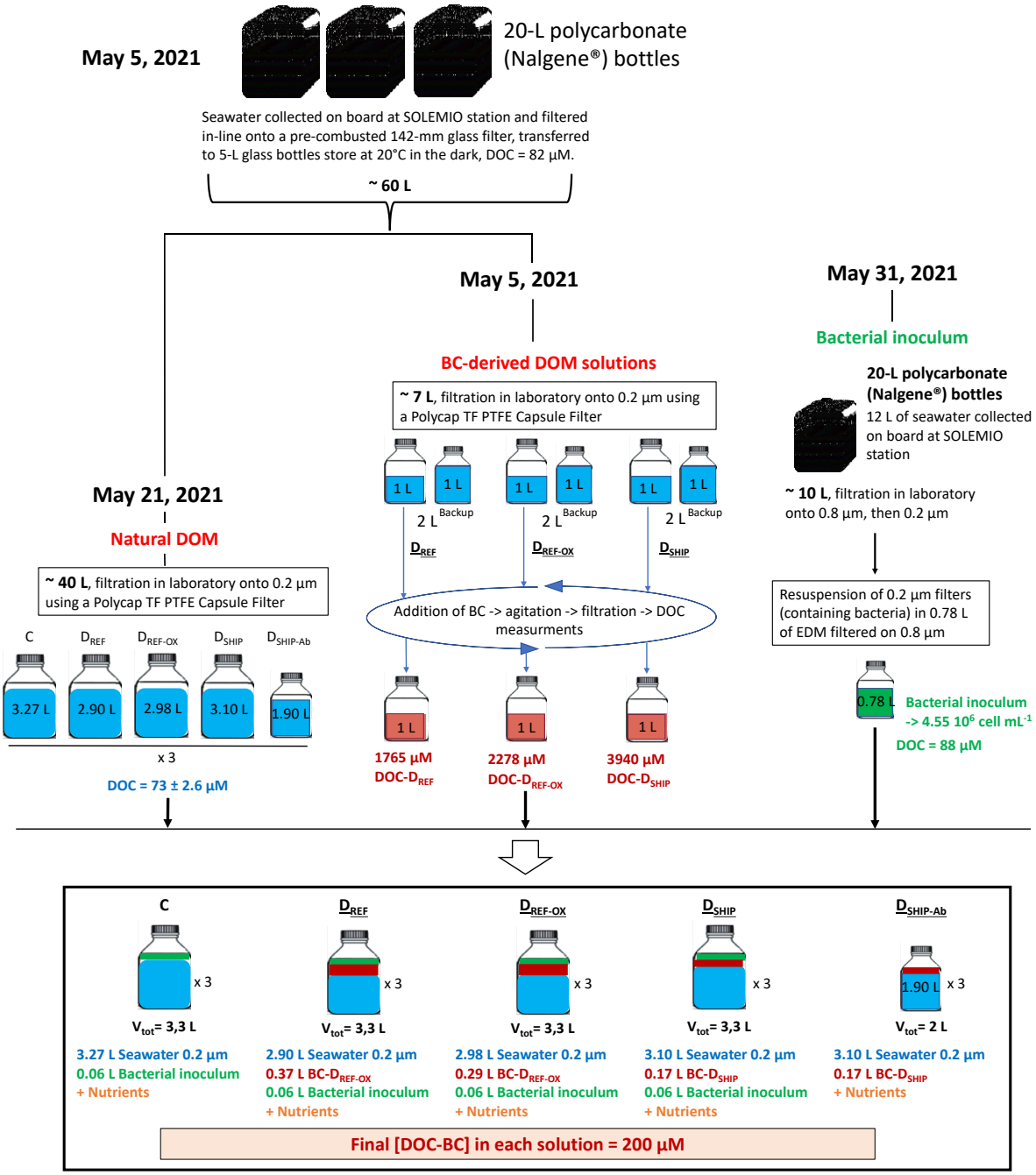


**Figure S2.** Diagram summarizing the preparation of the different solutions used to conduct the 90-day biodegradation experiment of the Black Carbon (BC)-derived dissolved organic matter (DOM) by marine heterotrophic prokaryotes, i.e., the natural DOM, the BC-derived DOM stock solutions and finally the incubation solutions for the five treatments in triplicates (giving 15 incubation bottles): C (control), $D_{REF}$ (diesel), $D_{REF\text{-}OX}$ (diesel oxidized), $D_{SHIP}$ (ship soot collected in the Haiphong harbor, Vietnam) and $D_{SHIP\text{-}Ab}$ ("abiotic" condition with ship soot).

**Table S1.** Concentrations in dissolved organic carbon (DOC), silicates [$Si(OH)_4$], nitrates ($NO_3^-$), nitrites ($NO_2^-$), ammonium ($NH_4^+$) and phosphates ($PO_4^{3-}$) determined in the different seawater solutions used for the preparation of the incubation solutions.

| **Type of solution** | **Date of preparation (in 2021)** | **Volume (L)** | **DOC (µM)** | **$Si(OH)_4$ (µM)** | **$NO_3^-$ (µM)** | **$NO_2^-$ (µM)** | **$NH_4^+$ (µM)** | **$PO_4^{3-}$ (µM)** |
|---|---|---|---|---|---|---|---|---|
| Seawater collected and filtered in-line onto GF/F (~ 0.7 µm) on board the R/V *Antédon 2* | May 5 | 60 | 80 | *nd* | *nd* | *nd* | *nd* | *nd* |
| Seawater (filtrate GF/F) filtered onto 0.2 µm in the lab for the preparation of the BC-derived DOM stock solutions | May 5 | 6 | 82 | *nd* | *nd* | *nd* | *nd* | *nd* |
| Seawater (filtrate GF/F) filtered onto 0.2 µm in the lab and used as natural marine DOM for the four biotic treatments | May 21 | 40 | 70-75 | 5.2-6.8 | 0.002-0.020 | 0.001-0.003 | 0.000-0.017 | 0.025-0.034 |
| BC-derived DOM stock solution from Diesel Particulate Matter particles ("$D_{REF}$") | May 18 | 1 | 1763* | 15.1 | 1.93 | 1.58 | 0.35 | 1.30 |
| BC-derived DOM stock solution from Diesel particles oxidized ("$D_{REF\text{-}OX}$") | May 18 | 1 | 2276* | 11.1 | 1.36 | 0.85 | 0.52 | 0.78 |
| BC-derived DOM stock solution from ship soot collected in Haiphong harbor, Vietnam ("$D_{SHIP}$") | May 18 | 1 | 3938* | 9.9 | 1.03 | 0.49 | 0.54 | 0.40 |
| 0.8-µm filtered seawater enriched with four 0.2-µm filters, over which were passed 10 L of seawater previously filtered onto 0.8 µm, and used as the natural prokaryotic assemblage solution (concentrated bacterial inoculum; $4.5.10^6$ cell $mL^{-1}$) | May 31 | 0.780 | 88 | *nd* | *nd* | *nd* | *nd* | *nd* |

*nd*: not determined.

* DOC concentrations related to the Black Carbon addition (DOC-BC), i.e., without taking into account the 82 µM DOC of the natural DOM used to make the BC-derived DOM stock solution.

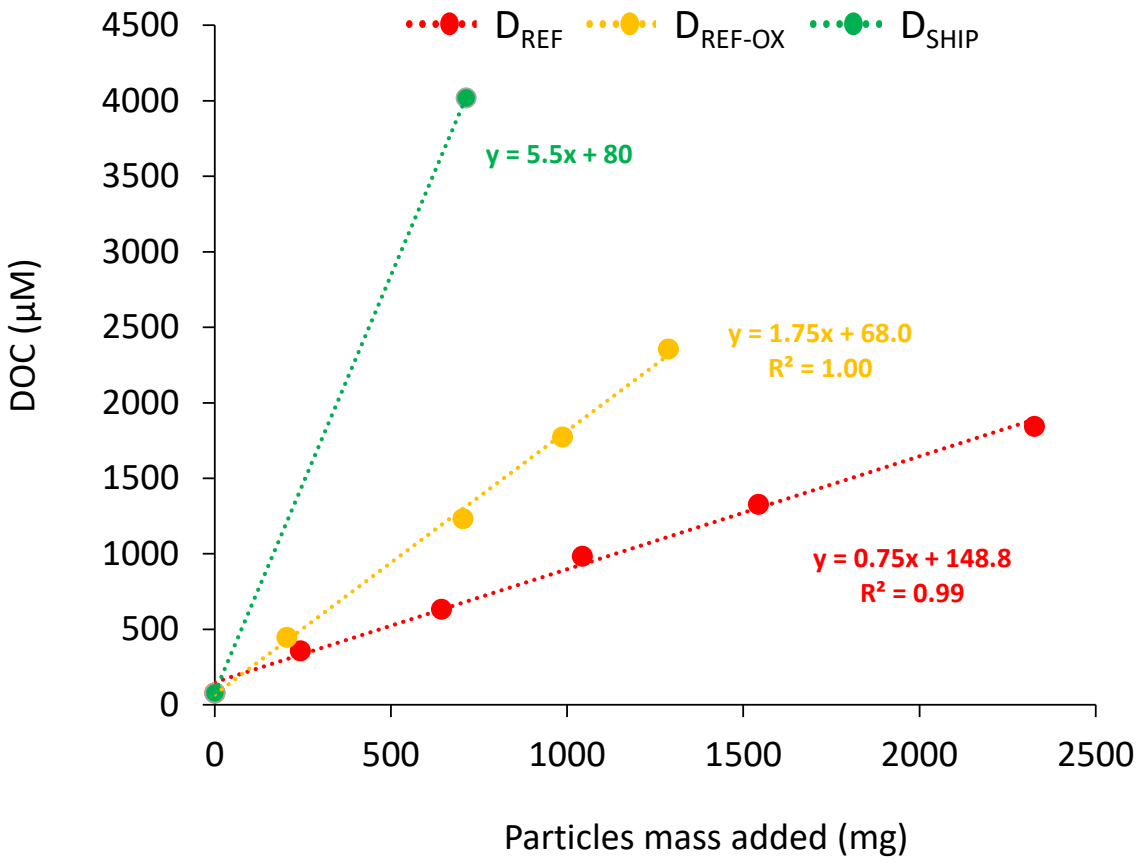


**Figure S3.** Relationship between the mass of soot particles added to the 1 L seawater solution (in mg) and the concentration of dissolved organic carbon (DOC in µM) in this solution after solubilization of the particles by ultrasonic bath and filtration on glass fiber filter (GF/F) for the three different Black Carbon (BC)-type materials: Diesel Particulate Matter reference material ($D_{REF}$), D particles that have been oxidized before use ($D_{REF\text{-}OX}$), and soot collected in February 2021 in the funnel of a ship moored in the Haiphong harbor in Vietnam ($D_{SHIP}$). These relationships illustrate the fact that $D_{SHIP}$ particles were much more water-soluble than $D_{REF}$ and $D_{REF\text{-}OX}$ particles, even though $D_{REF\text{-}OX}$ particles, due to their oxidation, were significantly more water-soluble than $D_{REF}$ particles.

**Table S2.** Theoretical final concentrations in dissolved organic carbon (DOC), silicates [$Si(OH)_4$], nitrates ($NO_3^-$), nitrites ($NO_2^-$), ammonium ($NH_4^+$) and phosphates ($PO_4^{3-}$) in the incubation solutions used for the 90-day biodegradation experiment. These concentrations were calculated from concentrations reported in Table S1 and volumes reported Table 1. C: control treatment (without BC-derived DOM); $D_{REF}$: Diesel Particulate Matter reference material; $D_{REF\text{-}OX}$: D particles that have been oxidized before use; $D_{SHIP}$: soot collected in February 2021 in the funnel of a ship moored in the Haiphong harbor in Vietnam. $D_{SHIP\text{-}Ab}$: "abiotic" condition with ship soot.

| **Final concentrations in µM** | **C** | **$D_{REF}$** | **$D_{REF\text{-}OX}$** | **$D_{SHIP}$** | **$D_{SHIP\text{-}Ab}$** |
|---|---|---|---|---|---|
| Total DOC | 73 | 270 | 272 | 275 | 270 |
| BC-derived DOC | 0 | 196 | 198 | 201 | 197 |
| Natural DOM-derived DOC | 72 | 73 | 72 | 72 | 73 |
| Bacterial inoculum-derived DOC | 2 | 2 | 2 | 2 | 0 |
| Total $Si(OH)_4$ | 5.97 | 6.98 | 6.41 | 6.17 | 6.17 |
| Total $NO_3^-$ | 11.71 | 6.49 | 7.42 | 9.20 | 9.28 |
| Total $NO_2^-$ | 0.002 | 0.178 | 0.075 | 0.027 | 0.026 |
| Total $NH_4^+$ | 0.007 | 0.045 | 0.052 | 0.034 | 0.034 |
| Total $PO_4^{3-}$ | 1.741 | 0.171 | 0.966 | 1.519 | 1.533 |

**Table S3.** Summary of the chemical and microbiological parameters measured on water sampled in the incubation solutions at each time (T0-T6) and for each treatment: C = 1, $D_{REF}$ = 2, $D_{REF\text{-}OX}$ = 3, $D_{SHIP}$ = 4, and $D_{SHIP\text{-}Ab}$ = 5.

| Point | **T0** | | | | | **T1** | | | | | **T2** | | | | | **T3** | | | | | **T4** | | | | | **T5** | | | | | **T6** | | | | |
|---|---|---|---|---|---|---|---|---|---|---|---|---|---|---|---|---|---|---|---|---|---|---|---|---|---|---|---|---|---|---|---|---|---|---|
| Days | 0 | | | | | 1 | | | | | 2 | | | | | 3 | | | | | 7 | | | | | 30 | | | | | 90 | | | | |
| Date | June 1, 2021 | | | | | June 2, 2021 | | | | | June 3, 2021 | | | | | June 4, 2021 | | | | | June 8, 2021 | | | | | June 29, 2021 | | | | | August 31, 2021 | | | | |
| | 1 | 2 | 3 | 4 | 5 | 1 | 2 | 3 | 4 | 5 | 1 | 2 | 3 | 4 | 5 | 1 | 2 | 3 | 4 | 5 | 1 | 2 | 3 | 4 | 5 | 1 | 2 | 3 | 4 | 5 | 1 | 2 | 3 | 4 | 5 |
| DOC | ✓ | ✓ | ✓ | ✓ | ✓ | ✓ | ✓ | ✓ | ✓ | ✓ | ✓ | ✓ | ✓ | ✓ | ✓ | ✓ | ✓ | ✓ | ✓ | ✓ | ✓ | ✓ | ✓ | ✓ | ✓ | ✓ | ✓ | ✓ | ✓ | ✓ | ✓ | ✓ | ✓ | ✓ | ✓ |
| DON | ✓ | ✓ | ✓ | ✓ | ✓ | | | | | | | | | | | | | | | | | | | | | | | | | | ✓ | ✓ | ✓ | ✓ | ✓ |
| DOP | ✓ | ✓ | ✓ | ✓ | ✓ | | | | | | | | | | | | | | | | | | | | | | | | | | ✓ | ✓ | ✓ | ✓ | ✓ |
| CDOM | ✓ | ✓ | ✓ | ✓ | ✓ | ✓ | ✓ | ✓ | ✓ | ✓ | ✓ | ✓ | ✓ | ✓ | ✓ | ✓ | ✓ | ✓ | ✓ | ✓ | ✓ | ✓ | ✓ | ✓ | ✓ | ✓ | ✓ | ✓ | ✓ | ✓ | ✓ | ✓ | ✓ | ✓ | ✓ |
| FDOM | ✓ | ✓ | ✓ | ✓ | ✓ | ✓ | ✓ | ✓ | ✓ | ✓ | ✓ | ✓ | ✓ | ✓ | ✓ | ✓ | ✓ | ✓ | ✓ | ✓ | ✓ | ✓ | ✓ | ✓ | ✓ | ✓ | ✓ | ✓ | ✓ | ✓ | ✓ | ✓ | ✓ | ✓ | ✓ |
| DBC | ✓ | ✓ | ✓ | ✓ | ✓ | | | | | | | | | | | | | | | | | | | | | | | | | | ✓ | ✓ | ✓ | ✓ | ✓ |
| d-PAHs | ✓ | ✓ | ✓ | ✓ | ✓ | | | | | | | | | | | | | | | | | | | | | | | | | | ✓ | ✓ | ✓ | ✓ | ✓ |
| NUT | ✓ | ✓ | ✓ | ✓ | ✓ | | | | | | | | | | | ✓ | ✓ | ✓ | ✓ | ✓ | | | | | | | | | | | ✓ | ✓ | ✓ | ✓ | ✓ |
| d-MTEs | ✓ | ✓ | ✓ | ✓ | ✓ | | | | | | | | | | | ✓ | ✓ | ✓ | ✓ | ✓ | | | | | | | | | | | ✓ | ✓ | ✓ | ✓ | ✓ |
| BA | ✓ | ✓ | ✓ | ✓ | ✓ | ✓ | ✓ | ✓ | ✓ | ✓ | ✓ | ✓ | ✓ | ✓ | ✓ | ✓ | ✓ | ✓ | ✓ | ✓ | ✓ | ✓ | ✓ | ✓ | ✓ | ✓ | ✓ | ✓ | ✓ | ✓ | ✓ | ✓ | ✓ | ✓ | ✓ |
| BP | ✓ | ✓ | ✓ | ✓ | ✓ | ✓ | ✓ | ✓ | ✓ | ✓ | ✓ | ✓ | ✓ | ✓ | ✓ | ✓ | ✓ | ✓ | ✓ | ✓ | ✓ | ✓ | ✓ | ✓ | ✓ | ✓ | ✓ | ✓ | ✓ | ✓ | ✓ | ✓ | ✓ | ✓ | ✓ |
| BR | ✓ | ✓ | ✓ | ✓ | | ✓ | ✓ | ✓ | ✓ | | ✓ | ✓ | ✓ | ✓ | | ✓ | ✓ | ✓ | ✓ | | ✓ | ✓ | ✓ | ✓ | | ✓ | ✓ | ✓ | ✓ | | ✓ | ✓ | ✓ | ✓ | |
| BD | ✓ | ✓ | ✓ | ✓ | ✓ | | | | | | | | | | | ✓ | ✓ | ✓ | ✓ | | | | | | | | | | | | ✓ | ✓ | ✓ | ✓ | ✓ |
| Nano | | | | | | | | | | | | | | | | ✓ | ✓ | ✓ | ✓ | | ✓ | ✓ | ✓ | ✓ | | ✓ | ✓ | ✓ | ✓ | | ✓ | ✓ | ✓ | ✓ | |

DOC: dissolved organic carbon; DON: dissolved organic nitrogen; DOP: dissolved organic phosphorous; CDOM: chromophoric dissolved organic matter; FDOM: fluorescent dissolved organic matter; DBC: dissolved Black Carbon; d-PAHs: dissolved polycyclic aromatic hydrocarbons; NUT: dissolved inorganic nutrients [silicates [$Si(OH)_4$], nitrates ($NO_3^-$), nitrites ($NO_2^-$), ammonium ($NH_4^+$) and phosphates ($PO_4^{3-}$)]; d-TM: dissolved metallic trace elements; BA: bacterial abundance; BP: bacterial production; BR: bacterial respiration; BD: bacterial diversity; Nano: abundance of heterotrophic nanoflagellates.

**Table S4.** Volume and filtration type used for the chemical and microbiological parameters measured on water sampled in the incubation solutions at each time and for each treatment. See definition of abbreviations in Table S3.

| | **Volume (mL)** | **Filtration** |
|---|---|---|
| DOC | 20 | GF/F filters (~ 0.7 µm), 47-mm diameter |
| DON + DOP | 70 | |
| CDOM + FDOM | 25 | |
| DBC + d-PAHs | 450 | |
| NUT | 60 | |
| d-TM | 30 | PES filters (0.2 µm), 25-mm-diameter |
| BA | ~ 2 | No filtration |
| BP | 10 | |
| BR | 7 | |
| BD | 400 | |
| Nano | ~ 2 | |

***Text 1. Dissolved inorganic nutrients.*** GF/F-filtered samples were transferred into 50-mL clean polycarbonate vials and stored at -20°C for a few days before analysis. $Si(OH)_4$, $NO_3^-$, $NO_2^-$, $PO_4^{3-}$ were analyzed by standard automated colorimetry procedure, using a Seal Analytical continuous-flow AutoAnalyzer III (AA3) as per the protocol given by Aminot and Kérouel (2004, 2007). $NH_4^+$ was analyzed by fluorescence as per Holmes et al. (1999) and Taylor et al. (2007). The detection limits of these ions were between 0.02 and 0.05 µM.

**Text 2.** ***Dissolved organic nitrogen and phosphorous (DON and DOP).*** GF/F-filtered samples were transferred into 100-mL pre-combusted glass vials and stored at -20°C for a few days before analysis. TDON (total dissolved organic nitrogen) and TDOP (total dissolved organic phosphorus) were determined by colorimetry after persulfate wet-chemical oxidation (Raimbault et al., 1999). DON and DOP were estimated after subtracting the dissolved inorganic fraction of nitrogen (DIN: $NO_3^- + NO_3^- + NH_4^+$) and phosphorus (DIP: $PO_4^{3-}$) from the total dissolved fractions (TDN and TDP).

***Text 3. Dissolved metallic trace elements (d-TM).*** 0.2-µm-filtered samples were transferred into clean 60-mL FEP vials, acidified (ultrapure HCl, pH 1), and stored at 4°C until analysis. Concentrations of d-TMs, i.e. aluminum (Al), vanadium (V), chromium (Cr), iron (Fe), cobalt (Co), nickel (Ni), copper (Cu), zinc (Zn), arsenic (As), antimony (Sb), lead (Pb), and uranium (U), were measured directly by argon gas dilution–inductively coupled plasma–mass spectrometry (iCAP-Q, Thermo Scientific) after acidification (ultrapure $HNO_3$ 1%v/v) using indium as internal standard for mass drift correction (Field et al., 1999; Quéméneur et al., 2020). Blanks and certified seawater samples (CASS-6) were analyzed following the same protocol to assess the efficiency of the method. Blanks were below the detection limit, and CASS-6 recovery was 100 ± 15% except for Cr (132%) and V (142%).

**Table S5.** Evolution of bacterial growth efficiency (BGE, %) calculated from respiration and bacterial production measurements throughout (1st (T1), 2nd (T2), 3rd (T3), 7th (T4), 30th (T5) and 90th day (T6)) in each biotic treatments: $D_{REF}$ (diesel), $D_{REF-OX}$ (diesel oxidized), $D_{SHIP}$ (ship soot) and C (control).

| | | C | | | $D_{REF}$ | | | $D_{REF-OX}$ | | | $D_{SHIP}$ | | |
|---|---|---|---|---|---|---|---|---|---|---|---|---|---|
| *Exponential phase* | T0 | 3.58 | ± | 0.10 | 4.70 | ± | 1.74 | 3.42 | ± | 0.02 | 3.95 | ± | 1.24 |
| | T1 | 4.66 | ± | 0.18 | 8.92 | ± | 2.12 | 8.88 | ± | 0.83 | 5.86 | ± | 0.01 |
| | T2 | 5.76 | ± | 0.62 | 11.69 | ± | 0.94 | 13.56 | ± | 0.38 | 10.41 | ± | 1.11 |
| | T3 | 5.01 | ± | 0.03 | 11.74 | ± | 0.19 | 13.68 | ± | 0.15 | 9.42 | ± | 1.15 |
| | T4 | 6.26 | ± | 0.08 | 8.90 | ± | 0.80 | 8.44 | ± | 0.40 | 6.21 | ± | 0.56 |
| | T5 | 3.34 | ± | 0.54 | 5.20 | ± | 0.20 | 6.25 | ± | 0.59 | 5.66 | ± | 0.18 |
| | T6 | 1.56 | ± | 0.19 | 2.70 | ± | 0.14 | 3.43 | ± | 0.74 | 2.83 | ± | 0.12 |

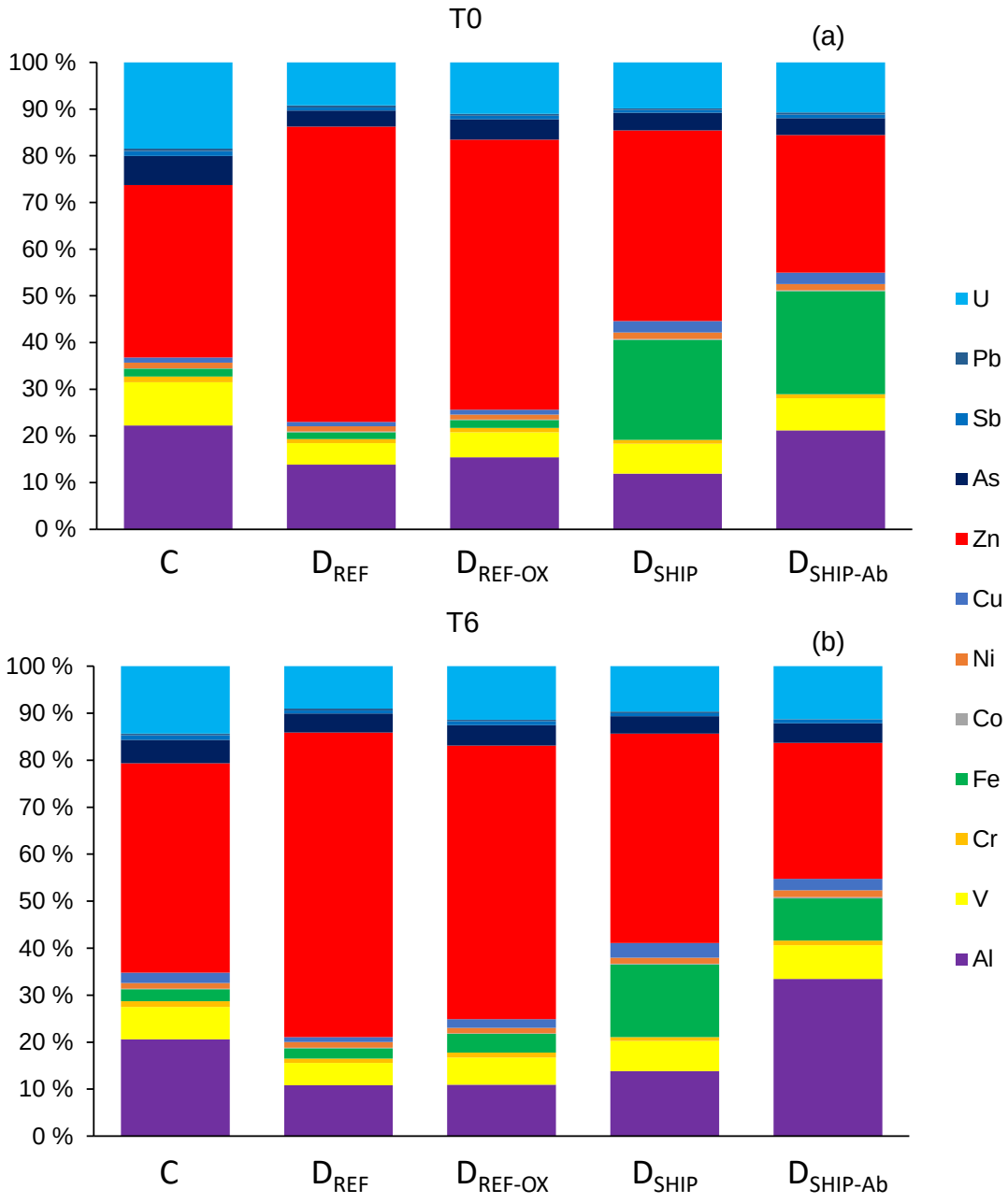


**Figure S4.** Relative abundances (in %) of dissolved metallic trace elements (d-TM) at the start (T0) (a) and the end (T6: 90 days) (b) of the biodegradation experiment for the four biotic treatments: C (control), $D_{REF}$ (diesel), $D_{REF\text{-}OX}$ (diesel oxidized), $D_{SHIP}$ (ship soot), and $D_{SHIP\text{-}Ab}$ ("abiotic" ship soot).

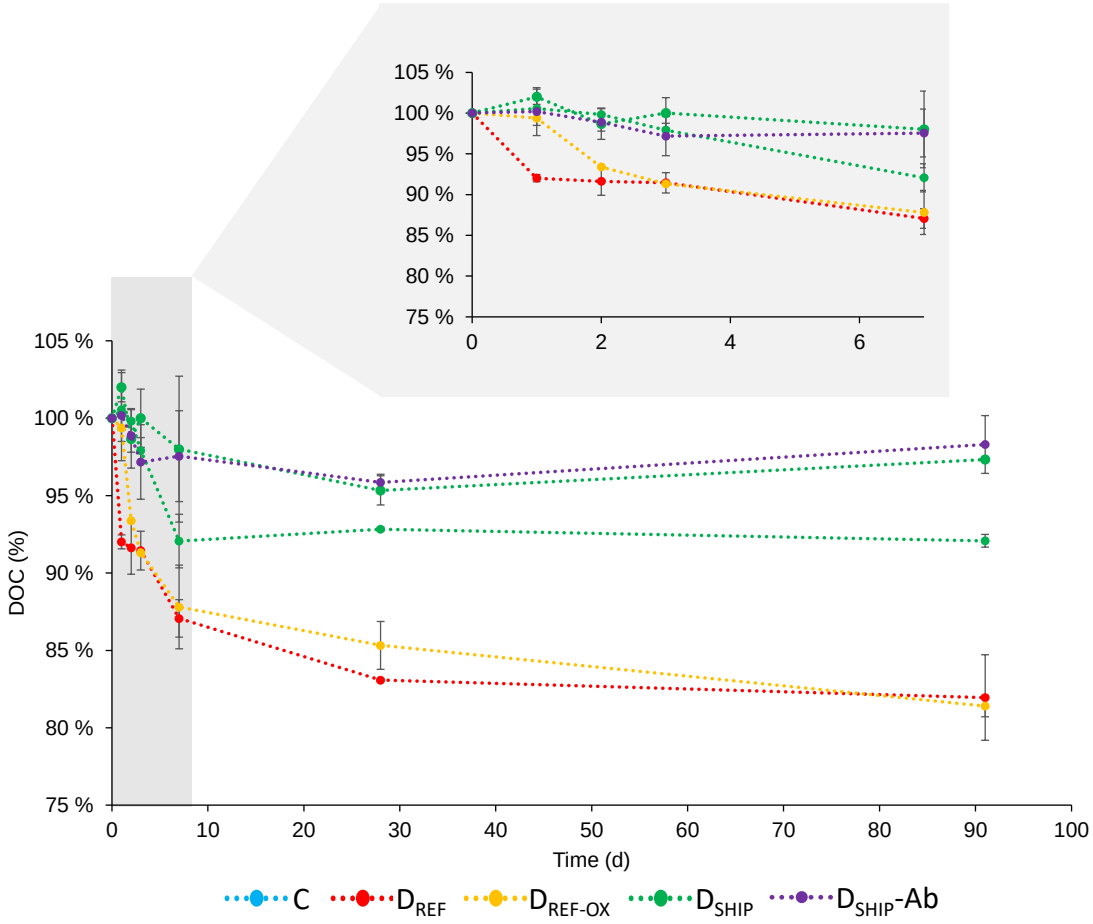


**Figure S5.** Evolution of dissolved organic carbon (DOC) in % relative to the initial concentration at T0 (100%) (c, d), throughout (up to T6: 90 days) (a, c) or during the first 7 days (up to T4: 7 days) (b, d) of the BC-derived DOM biodegradation experiment for the four biotic treatments: C (control), $D_{REF}$ (diesel), $D_{REF\text{-}OX}$ (diesel oxidized), $D_{SHIP}$ (ship soot), and $D_{SHIP\text{-}Ab}$ ("abiotic" ship soot). Error bars corresponds to the standard deviation of the triplicates.

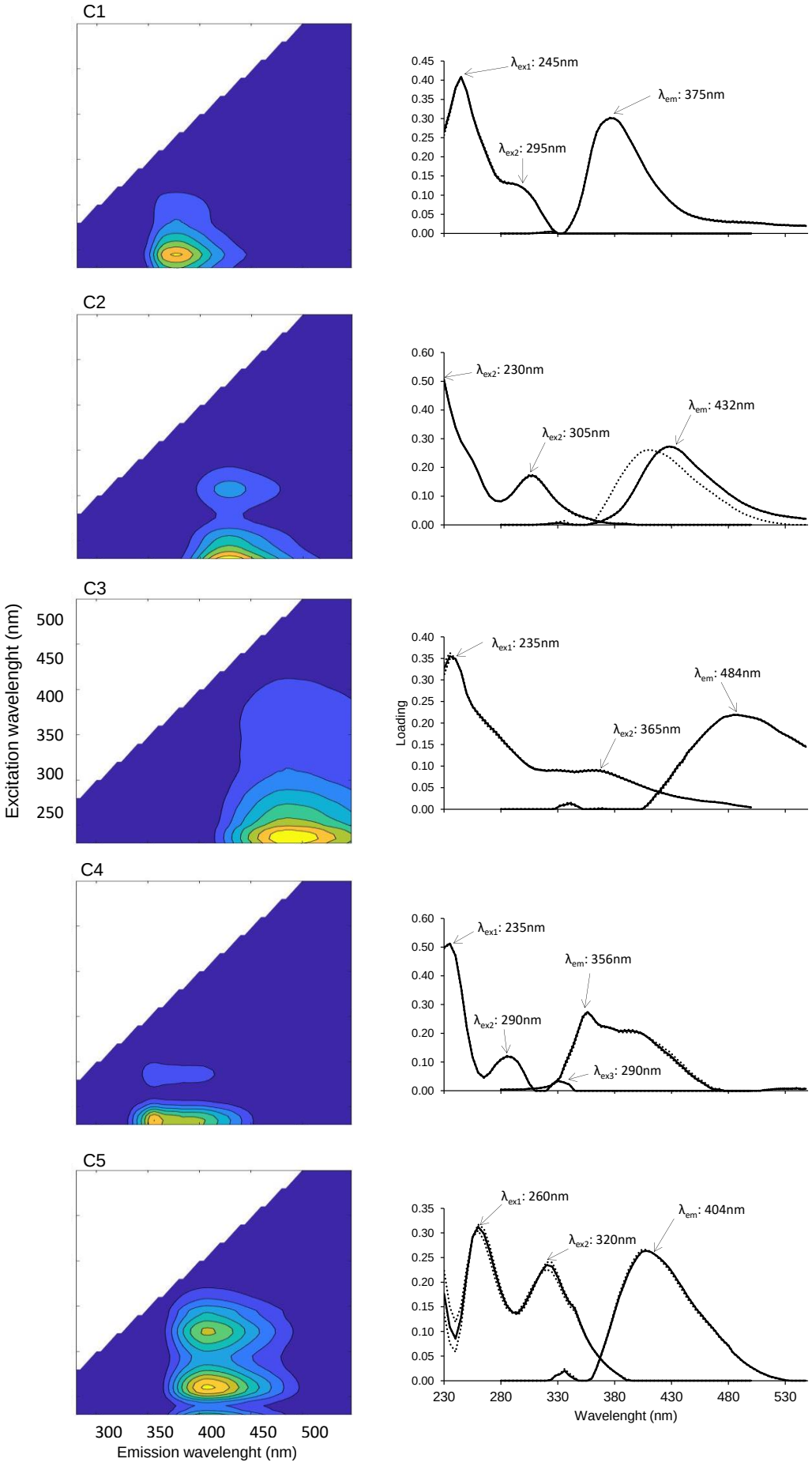
C1
λex1: 245nm
λem: 375nm
λex2: 295nm
C2
λex2: 230nm
λem: 432nm
λex2: 305nm
C3
λex1: 235nm
λem: 484nm
λex2: 365nm
Loading
C4
λex1: 235nm
λem: 356nm
λex2: 290nm
λex3: 290nm
C5
λex1: 260nm
λem: 404nm
λex2: 320nm
Excitation wavelenght (nm)
Emission wavelenght (nm)
Wavelenght (nm)

**Figure S6.** Spectral characteristics of the five FDOM components (C1-C5) validated by the PARAFAC model for 105 EEMs of samples collected throughout the biodegradation experiment (from T0 to T6) for the different BC treatments ($D_{REF}$, $D_{REF\text{-}OX}$ and $D_{SHIP}$). The line plots show the excitation (left side) and emission (right side) fluorescence spectra. The dotted lines correspond to split half validation results. The excitation and emission maxima ($\lambda_{Ex}$ and $\lambda_{Em}$) of each component are given.

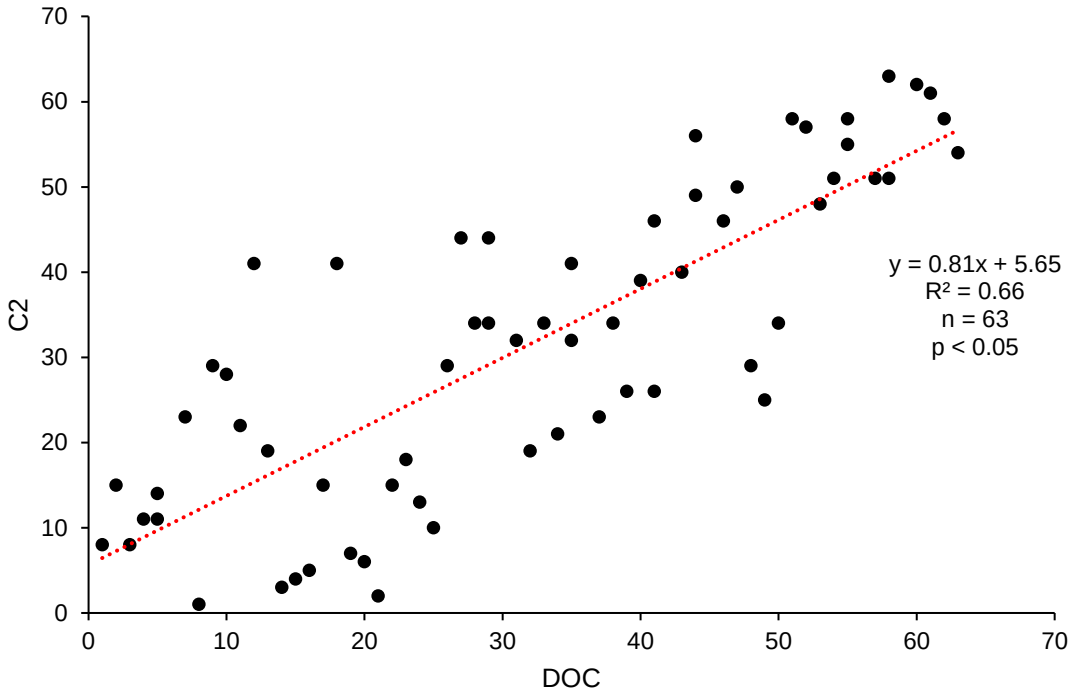


**Figure S7.** Spearman correlation between the concentration of dissolved organic carbon (DOC, in µM) and the fluorescence intensity of C2 FDOM component (in QSU, $\lambda_{Ex}/\lambda_{Em}$: 305/432 nm), over the course of the biodegradation experiment, all times (from T0 to T6) and BC treatments ($D_{REF}$, $D_{REF\text{-}OX}$ and $D_{SHIP}$) combined (n = 63).

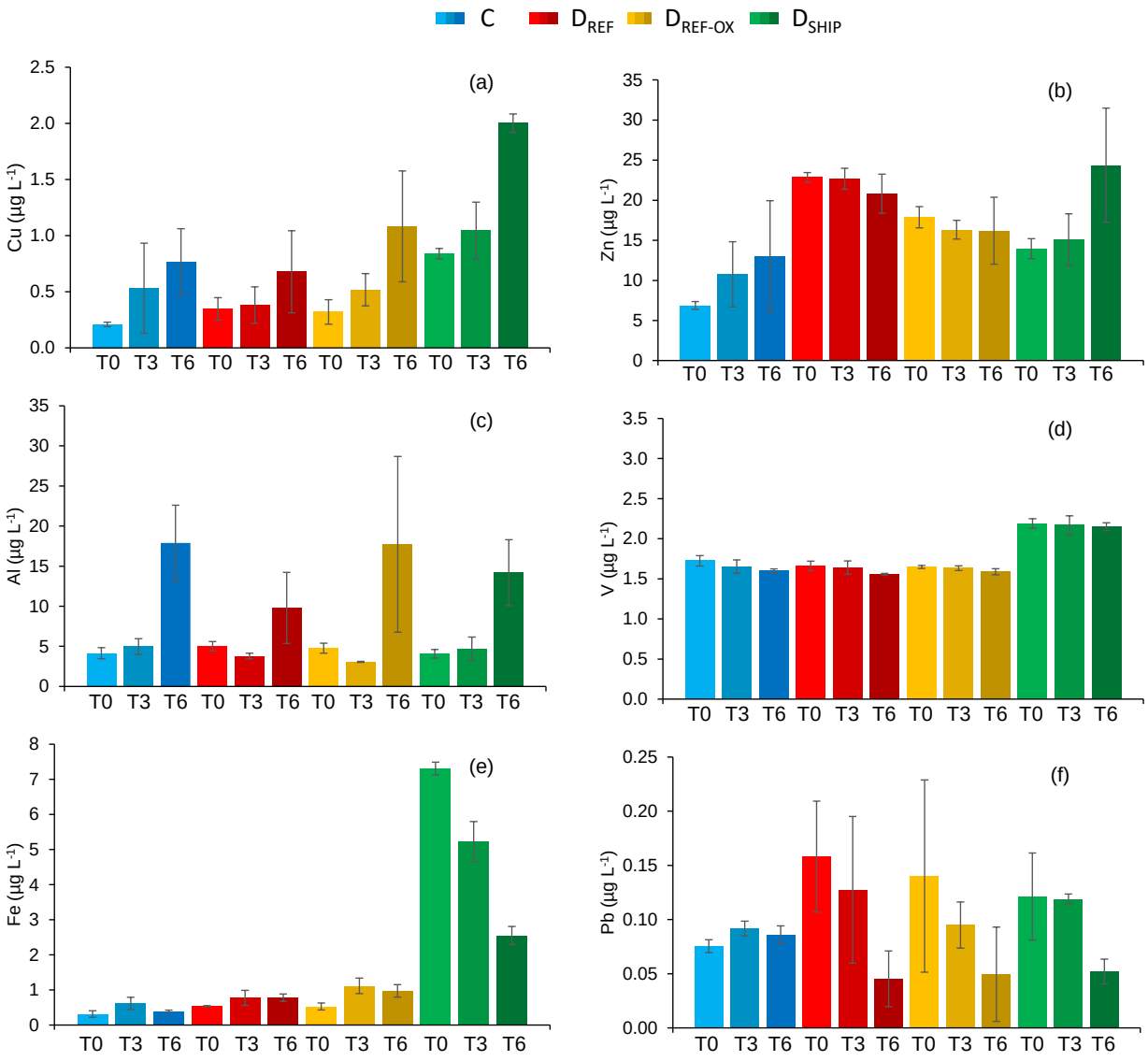


**Figure S8.** Concentrations of several individual dissolved metallic trace elements (d-TM, in µg $L^{-1}$) at the start (T0), after 3 days (T3) and at the end (T6: 90 days) of the biodegradation experiment: copper (Cu) (a), zinc (Zn) (b), aluminum (Al) (c), vanadium (V) (d), iron (Fe) (e) and lead (Pb) (f), for the four biotic treatments: C (control), $D_{REF}$ (diesel), $D_{REF\text{-}OX}$ (diesel oxidized), and $D_{SHIP}$ (ship soot). Error bars corresponds to the standard deviation of the triplicates.

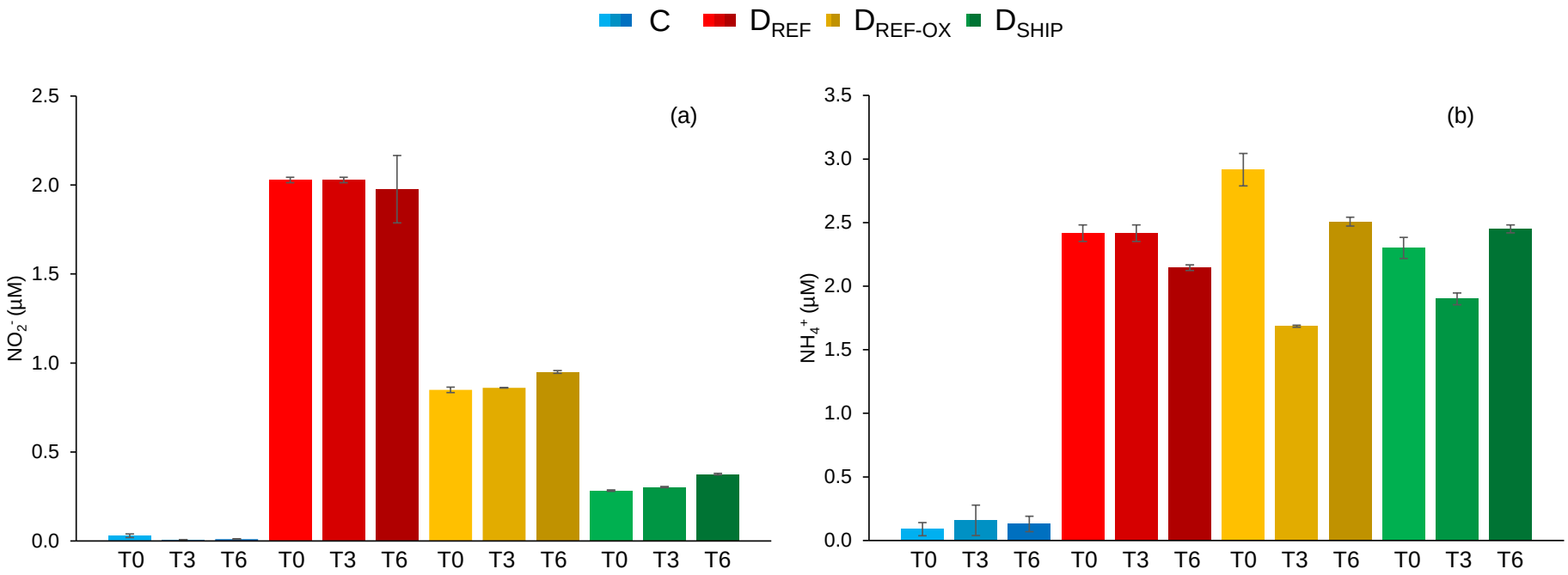


**Figure S9.** Concentrations of dissolved organic nitrogen (DON, in µM) (a) and dissolved organic phosphorus (DOP, in µM) (b) at the start (T0) and the end (T6: 90 days) of the biodegradation experiment for the four biotic treatments: C (control), $D_{REF}$ (diesel), $D_{REF\text{-}OX}$ (diesel oxidized), and $D_{SHIP}$ (ship soot). Error bars corresponds to the standard deviation of the triplicates.

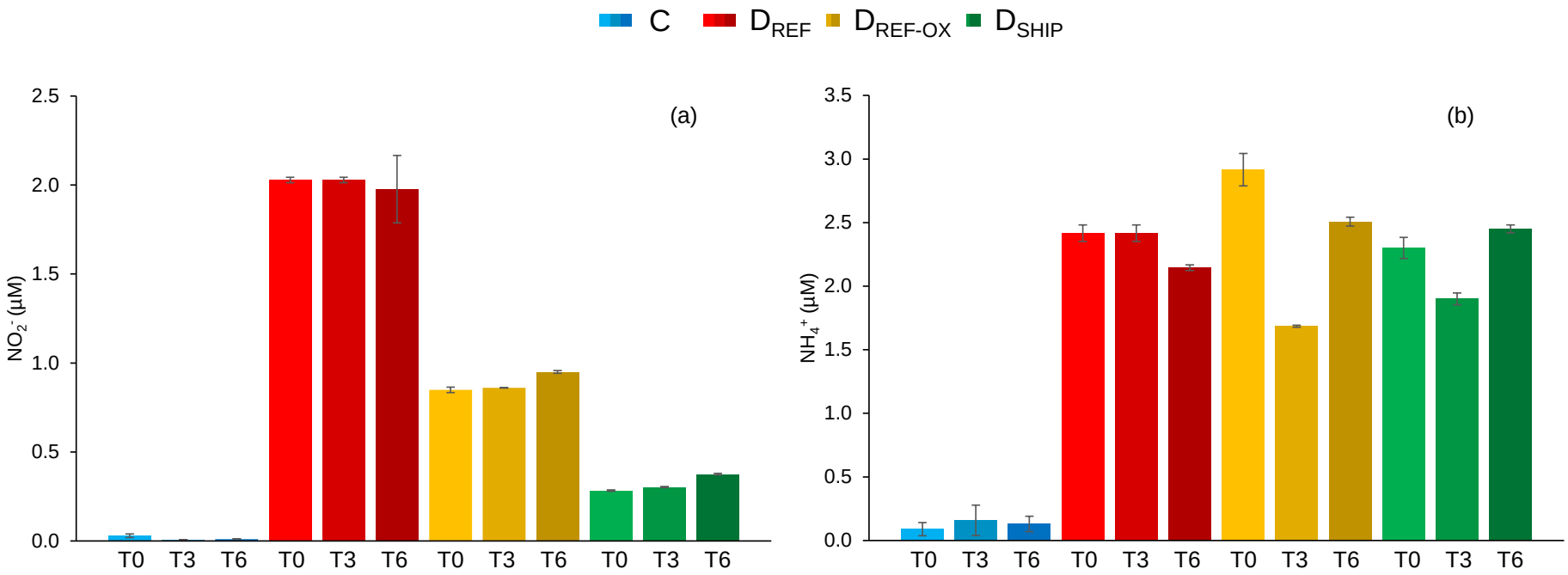


**Figure S10.** Concentrations of dissolved nitrites ($NO_2^-$, in µM) (a) and dissolved ammonium ($NH_4^+$, in µM) (b) at the start (T0), after 3 days (T3) and at the end (T6: 90 days) of the biodegradation experiment for the four biotic treatments: C (control), $D_{REF}$ (diesel), $D_{REF\text{-}OX}$ (diesel oxidized), and $D_{SHIP}$ (ship soot).

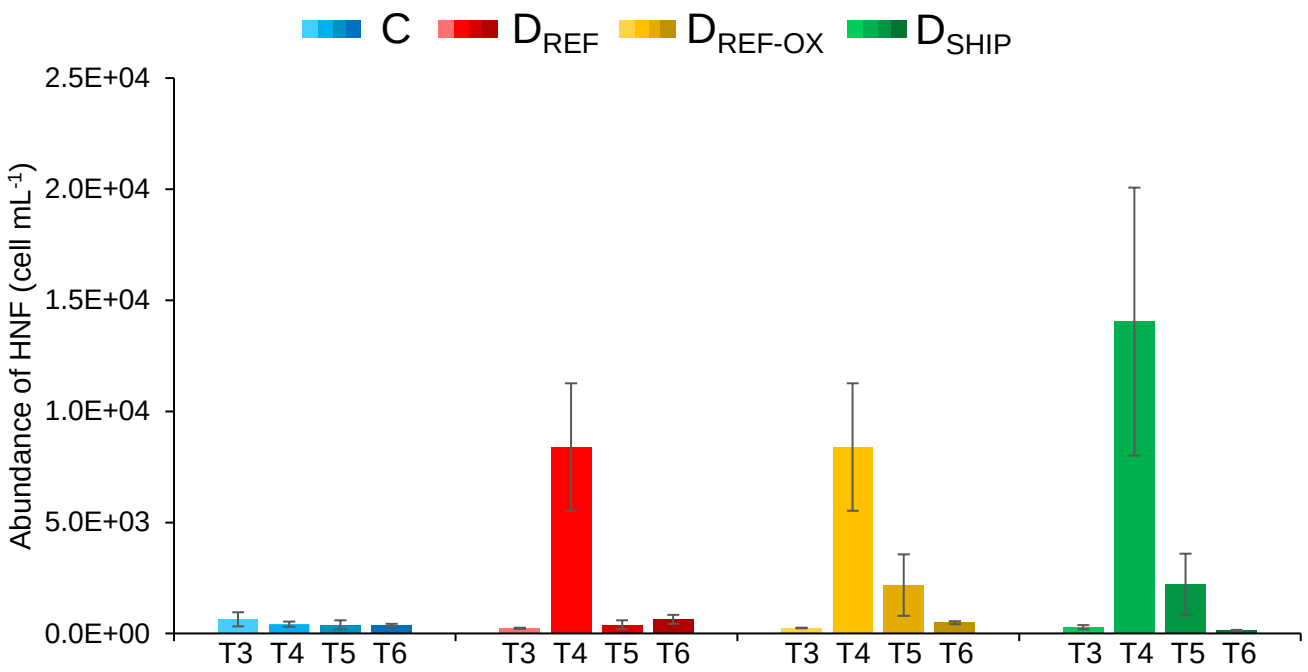


**Figure S11.** Concentrations of heterotrophic nanoflagellates (HNF, in cell $mL^{-1}$) after 3 days (T3), 7 days (T4), 28 days (T5) and at the end (T6: 90 days) of the biodegradation experiment for the four biotic treatments: C (control), $D_{REF}$ (diesel), $D_{REF\text{-}OX}$ (diesel oxidized), and $D_{SHIP}$ (ship soot). Error bars corresponds to the standard deviation of the triplicates.

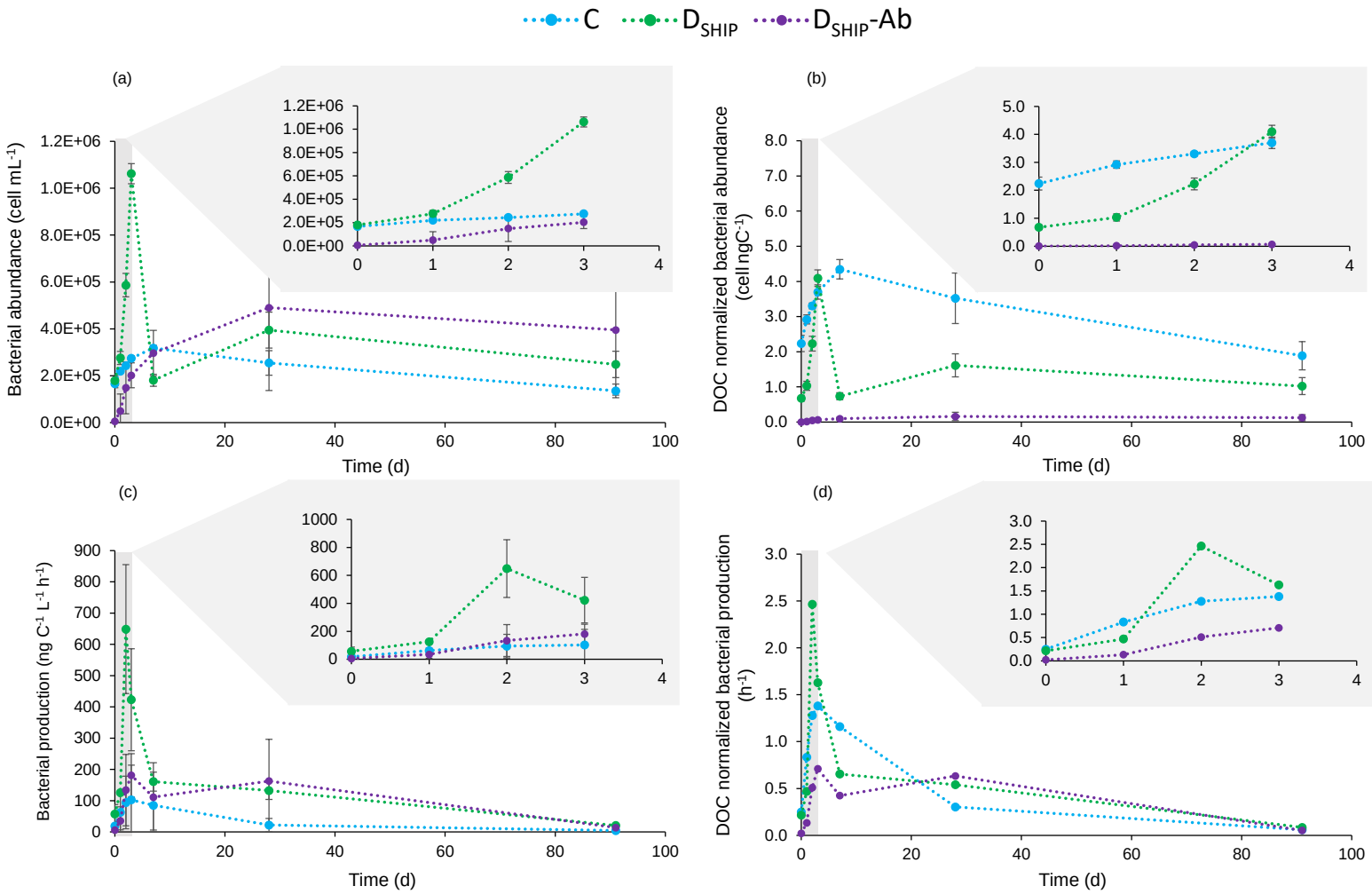


**Figure S12.**

Time-course of (a) bacterial abundance (cell $mL^{-1}$), (b) bacterial abundance normalized to DOC (cell ng $C^{-1}$), bacterial production (ng C $L^{-1}$ $h^{-1}$) and (c) bacterial production normalized to DOC ($h^{-1}$) (d) throughout the BC-derived DOM biodegradation experiment (up to T6: 90 days), with a

focus on the first 3 days (up to T3: 3 days), for C (control), $D_{SHIP}$ (ship soot) and $D_{SHIP}$-Ab (abiotic condition with ship soot). Error bars correspond to the standard deviation of the triplicates.

**Table S6.** BPCAs concentrations (μg C $L^{-1}$) measured in BC-derived DOM solutions at the start (T0) and the end (T6) of the biodegradation experiment for the four BC treatments: $D_{REF}$ (diesel), $D_{REF\text{-}OX}$ (oxidized diesel), $D_{SHIP}$ (ship soot), and $D_{SHIP\text{-}Ab}$ ("abiotic" ship soot). The values and degradation percentages are the average and standard deviation of the triplicates (three bottles) for each treatment. Values in bold indicate a statistically significant decrease (t-test, superscript a for $p \leq 0.05$ and superscript b for $p \leq 0.07$).

| | Treatments | T0 | T6 | Degradation (%) |
|---|---|---|---|---|
| B3CA | $D_{REF}$ | 1012 ± 86 | 623 ± 45 | **39.4**[a] ± 2.3 |
| | $D_{REF\text{-}OX}$ | 1048 ± 121 | 652 ± 17 | **37.2**[a] ± 7 |
| | $D_{SHIP}$ | 1457 ± 60 | 903 ± 20 | **38.0**[a] ± 2.4 |
| | $D_{SHIP\text{-}Ab}$ | 1374 ± 124 | 1212 ± 276 | 5 ± 8.4 |
| B4CA | $D_{REF}$ | 1704 ± 83 | 1105 ± 80 | **36.6**[a] ± 2 |
| | $D_{REF\text{-}OX}$ | 1742 ± 72 | 1120 ± 27 | **27.3**[b] ± 8.8 |
| | $D_{SHIP}$ | 1890 ± 181 | 1571 ± 12 | 16.4 ± 7.2 |
| | $D_{SHIP\text{-}Ab}$ | 1803 ± 370 | 1604 ± 17 | 8.4 ± 19.6 |
| B5CA | $D_{REF}$ | 900 ± 172 | 494 ± 11 | **49.6**[a] ± 7.1 |
| | $D_{REF\text{-}OX}$ | 780 ± 133 | 538 ± 41 | **30.2**[b] ± 7.1 |
| | $D_{SHIP}$ | 683 ± 110 | 655 ± 32 | 2.8 ± 11.6 |
| | $D_{SHIP\text{-}Ab}$ | 685 ± 175 | 602 ± 139 | 4.9 ± 44 |
| B6CA | $D_{REF}$ | 83 ± 5 | 57 ± 5 | **33**[a] ± 3.6 |
| | $D_{REF\text{-}OX}$ | 83 ± 2 | 69 ± 12 | 16.9 ± 14 |
| | $D_{SHIP}$ | 73 ± 12 | 80 ± 12 | 12.8 ± 29 |
| | $D_{SHIP\text{-}Ab}$ | 71 ± 15 | 66 ± 24 | -0.2 ± 49.9 |

**Table S7.** Concentrations of low-molecular-weight (LMW) and high-molecular-weight (HMW) PAHs (μg $L^{-1}$) measured in BC-derived DOM solutions at the start (T0) and the end (T6) of the biodegradation experiment for the four BC treatments: $D_{REF}$ (diesel), $D_{REF\text{-}OX}$ (oxidized diesel), and $D_{SHIP\text{-}Ab}$ ("abiotic" ship soot). The values and degradation percentages are the average and standard deviation of the triplicates (three bottles) for each treatment. Values in bold indicate a statistically significant decrease (t-test, $p \leq 0.1$).

| | Treatments | T0 | T6 | Degradation (%) |
|---|---|---|---|---|
| LMW | **$D_{REF}$** | 20 ± 8 | 7 ± 1 | **59.5** ± 14.5 |
| | **$D_{REF\text{-}OX}$** | 16 ± 4 | 4 ± 2 | **72** ± 17 |
| | **$D_{SHIP}$** | 297 ± 91 | 224 ± 55 | 23 ± 9.5 |
| | **$D_{SHIP\text{-}Ab}$** | 246 ± 68 | 253 ± 11 | -9.5 ± 33.5 |
| HMW | **$D_{REF}$** | 7 ± 2 | 4 ± 1 | **46** ± 10 |
| | **$D_{REF\text{-}OX}$** | 7 ± 3 | 4 ± 1 | 41.5 ± 12 |
| | **$D_{SHIP}$** | 12 ± 1 | 9 ± 1 | **20.5** ± 10 |
| | **$D_{SHIP\text{-}Ab}$** | 12 ± 1 | 16 ± 2 | -34 ± 24 |